Title

- **De novo synthesis and salvage pathway coordinately regulates polyamine homeostasis and determines T cell proliferation and function.**
- **Polyamine homeostasis determines T cell function.**

Authors

Ruohan Wu[1†], Xuyong Chen[1†], Siwen Kang[1†], Tingting Wang[1], JN Rashida Gnanaprakasam[1], Yufeng Yao[3], Lingling Liu[1], Song Guo Zheng[2], Gaofeng Fan[3], Mark R Burns[4] and Ruoning Wang[1]*

Affiliations

[1]Center for Childhood Cancer & Blood Diseases, Hematology/Oncology & BMT, Abigail Wexner Research Institute at Nationwide Children's Hospital, The Ohio State University, Columbus, OH, USA.

[2]Division of Rheumatology and Immunology, Department of Internal Medicine at Ohio State University of Medicine and Wexner Medical Center, Columbus, OH, USA.

[3]School of Life Science and Technology, ShanghaiTech University, Shanghai, China.

[4]Aminex Therapeutics Inc., Epsom, NH 03234, USA.

†Wu R, Chen X and Kang S contributed equally to this paper

*Correspondence should be addressed to:

Ruoning Wang, Phone: 614-335-2980; Fax: 614-722-5895.

ruoning.wang@nationwidechildrens.org;

Abstract

Robust and effective T cell-mediated immune responses require proper allocation of metabolic resources through metabolic pathways to sustain the energetically costly immune response. As an essential class of polycationic metabolites ubiquitously present in all living organisms, the polyamine pool is tightly regulated by biosynthesis and salvage pathway. We demonstrated that arginine is a major carbon donor and glutamine is a minor carbon donor for polyamine biosynthesis in T cells. Accordingly, the dependence of T cells can be partially relieved by replenishing the polyamine pool. In response to the blockage of de novo synthesis, T cells can rapidly restore the polyamine pool through a compensatory increase in polyamine uptake from the environment, indicating a layer of metabolic plasticity. Simultaneously blocking synthesis and uptake depletes the intracellular PA pool, inhibits T cell proliferation, suppresses T cell inflammation, indicating the potential therapeutic value of targeting the polyamine for managing inflammatory and autoimmune diseases.

Introduction

To cope with pathogens' capacity for exponential growth, T cells have evolved mechanisms for rapidly adjusting their metabolism in response to T cell receptor (TCR) activation and additional signals indicating environmental change. A robust and effective metabolic reprogramming enables T cells to rapidly expand in number and differentiate to achieve large numbers of effector cells specialized in producing high levels of cytokines. Emerging evidences have shown that metabolic rewiring of the central carbon metabolism maximizes the acquisition and assimilation of energy and carbon sources, and prepare T cells for growth, differentiation, immune regulation and defense (*1-5*). Glycolysis, the pentose phosphate pathway (PPP), the Krebs cycle and fatty acid oxidation (FAO) represent a core set of metabolic pathways that transform carbon and chemical energy from environmental nutrients to support the bioenergetic and biosynthesis needs of T cells. Beyond that, a myriad of peripheral metabolic pathways is integrated in complex metabolic networks and are tightly regulated to generate specialized metabolites, which are essential for maintaining homeostasis and immune functions of T cells.

Non-essential amino acids including arginine, glutamine, and proline have both anabolic and catabolic functions, providing building blocks for protein and nucleic acids, and connecting central carbon metabolism to a variety of specialized metabolic pathways, including polyamine biosynthesis (*6-9*). Polyamine is an essential class of polycationic metabolites ubiquitously present in all living organisms. In addition to de novo biosynthesis, other metabolic routes including polyamine catabolism, influx and efflux act in concert to determine the size of the intracellular polyamine pool (*10*). Disrupting polyamine homeostasis can affect a plethora of cellular processes, including differentiation, transcription, translation, redox balance, and mitochondria quality control (*10*). Dysregulation of the level of polyamine and its amino acid precursors has been found to be associated with inflammation and autoimmune diseases (*11, 12*). We have previously reported that polyamines are one of the most upregulated metabolite groups

following T cell activation, and transcription factor MYC is responsible for its upregulation (*13*). Emerging evidence has also shown that polyamine homeostasis is tightly regulated in cellular contexts other than T cells, which have critical roles in immune regulation and defense (*14-18*). As such, a better understanding of how polyamine homeostasis is regulated in immune cells will reveal the fundamental principles of the emerging connections between immune cell metabolic fitness and functional robustness. Further knowledge will also enable us to devise rational and practical approaches to treat inflammatory and autoimmune diseases.

Intrinsic T cell signaling cascades are instrumental in the control of T cell metabolic programming (*5, 19-23*). Numerous extrinsic environmental factors including oxygen and nutrient supplies also significantly influence T cell metabolic phenotypes and, thus, immune functions *in vivo* (*24*). Here, we report that the intracellular polyamine pool is tightly regulated by de novo biosynthesis and cellular uptake, through the import of extracellular polyamine. Heightened arginine and glutamine catabolism provide carbon sources to support polyamine de novo biosynthesis *in vitro*. Genetic and pharmacologic ablation of de novo biosynthesis of polyamine is sufficient to deplete the polyamine pool and suppress T cell proliferation *in vitro*. However, de novo biosynthesis is dispensable in driving T cell proliferation *in vivo* where T cells can salvage circulating polyamine to maintain intracellular polyamine pool. Simultaneously blocking polyamine synthesis and salvage inhibits T cell proliferation *in vivo* and confers protection against the pathogenic development of experimental autoimmune encephalomyelitis (EAE). Our findings implicate the potential therapeutic value of targeting the polyamine metabolism in treating and managing inflammatory and autoimmune diseases.

Results

Inhibition of ODC reduces T cell proliferation and viability *in vitro*

We previously reported that a Myc-dependent non-canonical metabolic pathway links amino acid catabolism to the biosynthesis of polyamines during T cell activation (*13*). To investigate the role of polyamine metabolism in T cells, we employed a genetic and a pharmacologic approach to ablate polyamine de novo biosynthesis. Since ornithine decarboxylase (ODC), the rate-limiting enzyme in polyamine de novo biosynthetic pathway, is essential for early embryo development, and ODC germline knockout is embryonically lethal (*25*), we obtained a mouse strain containing a reporter-tagged conditional allele of ODC (FRT-LacZ; ODC^{fl}) generated by the European Mouse Mutant Archive (*26*). We first crossed this strain with the FLP knock-in mouse strain, which removed the LacZ-reporter allele and generated the strain containing the conditional allele (ODC^{fl}). Then, we generated a T cell-specific ODC knockout strain (ODC cKO) by crossing the ODC^{fl} strain with the CD4-Cre strain. The deletion of ODC was validated by qPCR (Fig. S1A), and the ablation of polyamine de novo synthesis was further validated by the accumulation of ornithine (substrate of ODC) and the depletion of putrescine, N-Acetylputrescine, spermine, and spermidine (Fig. S1B). ODC deletion did not affect the distribution of T cell subsets in the thymus, spleen and lymph nodes (Fig. S2A and S2B). In addition, the percentage of naturally occurring IFN-γ-producing, IL-17-producing, and $FoxP3^{+}$ CD4 T cells is comparable in both WT and ODC cKO animals (Fig. S2C). However, genetic deletion of ODC significantly delayed cell cycle progression from G0/G1 to the S phase after T cell activation and suppressed overall T cell proliferation in vitro (Fig. 1A and 1B). Consistent with the impact of genetic deletion of ODC on T cells, difluoromethylornithine (DFMO), a

potent inhibitor of ODC, inhibited activation-induced T cell cycle progression and proliferation *in vitro* (Fig. 1C and 1D). Finally, both genetic deletion of ODC and DFMO treatment caused moderately more cell death after activation in a time-dependent manner (Fig. 1E and 1F). Together, our results indicate that polyamine homeostasis is critical for T cell proliferation and survival.

ODC activity is dispensable for T cell proliferation and function *in vivo*

Controlling polyamine homeostasis is crucial for supporting cellular functions in all cell types, and both de novo biosynthesis and salvage by importing extracellular polyamine into the cell tightly regulates cellular polyamine-pool size (*10*). Without exogenous polyamine supplements in cell culture media, we envisioned that T cells would solely depend on de novo biosynthesis to maintain the intracellular polyamine pool *in vitro*. However, circulating polyamines that are provided by dietary intake and by intestinal microbiota may be a source of exogenous polyamine for T cells *in vivo* (*27*). To assess the impact of ablating de novo biosynthesis on CD4 T cell proliferation *in vivo*, we employed a well-established competitive homeostatic proliferation assay to determine the ratio and carboxyfluorescein succinimidyl ester (CFSE) dilution pattern of purified WT(Thy1.1^{+}) or ODC cKO(Thy1.2^{+}) CD4^{+} T cells in Rag1-deficient (*Rag1*$^{-/-}$) mice which lack endogenous T cells and permit spontaneous proliferation of adoptively transferred donor T cells. Surprisingly, the ratio between WT and ODC cKO CD4^{+} T cells was similar before and after adoptive transfer. Additionally, WT and ODC cKO CD4^{+} T cells display an overlapped CFSE dilution pattern, indicating that the loss of ODC did not affect T cell proliferation *in vivo* (Fig. 2A). Next, we sought to measure antigen-specific, TCR-dependent proliferation of WT or ODC cKO CD4^{+} T cells. We crossed Thy1.1 and CD4-Cre, ODC^{fl} mice

with OT-II transgenic mice to generate WT(Thy1.1$^+$) and ODC cKO(Thy1.2$^+$) donor OT-II strains in CD45.2$^+$ background. We then adoptively transferred mixed and CFSE labelled WT and ODC cKO CD4$^+$ T cells into CD45.1$^+$ mice that were immunized with chicken ovalbumin 323-339 peptide ($OVA_{323-339}$) in complete Freund's adjuvant (CFA). After 7 days, we measured the percentage ratio and CFSE dilution pattern of WT(Thy1.1$^+$) and ODC cKO(Thy1.2$^+$) CD4$^+$ T cells in popliteal lymph node. Consistent with the homeostatic proliferation results, WT and ODC cKO OT-II specific CD4$^+$ T cells display a comparable antigen-specific proliferation (Fig. 2B). The expansion and balance between pro-inflammatory CD4$^+$ T effector (T_{eff}) cells determine the pathogenic development of experimental autoimmune encephalomyelitis (EAE), a murine model of multiple sclerosis (MS), which is an inflammatory demyelinating disease of the central nervous system (CNS). We employed this well-characterized system to further interrogate an *in vivo* CD4 T cell response in the absence of polyamine de novo biosynthesis. In line with our homeostatic and antigen-specific proliferation data, neither the genetic deletion of ODC in T cells nor the systemic delivery of DFMO changes the kinetics of pathogenic progression (Fig. 2C and 2D). Together, our data indicates that polyamine salvage from circulation may be able to support T cell proliferation and effector function by compensating for the loss of de novo biosynthesis in the *in vivo* environment.

Polyamine salvage compensates for the loss of biosynthesis activity *in vitro*

Next, we investigated the role of polyamine salvage (uptake) in regulating polyamine homeostasis in T cell. We measured polyamine uptake activity using radioactive-labelled putrescine (^{14}C-Putrescine) in naïve, active WT and ODC cKO T cells. Active T cells displayed higher polyamine uptake activity than naïve T cells (Fig. 3A). Importantly, ablation of ODC

induces a compensatory increase in polyamine uptake (Fig. 3B). Next, we asked if polyamine uptake is sufficient to maintain polyamine homeostasis and support T cell proliferation in the absence of ODC activity. While genetic deletion or pharmacologic inhibition of ODC significantly delayed cell cycle progression from G0/G1 to the S phase and suppressed overall T cell proliferation, exogenous polyamine supplement could restore the cell cycle progression, proliferation and viability in DFMO-treated and ODC cKO $CD4^+$ T cells *in vitro* (Fig. 3C-3F and Fig. S3A-S3B). We then sought to employ a pharmacologic approach to block polyamine uptake and assessed the role of polyamine uptake in regulating polyamine homeostasis. AMXT 1501 (AMXT) is a novel lipophilic polyamine mimetic that potently blocks polyamine uptake in the low nanomolar concentration (*28*). The combination of AMXT and DFMO could effectively deplete the polyamine pool in tumor cells and suppress the growth of tumors (*29*). These promising preclinical studies led to a recently opened Phase I clinical trial in solid tumors (NCT03077477). Similar to the genetic data (Fig. 3B), DFMO treatment induces a compensatory increase in polyamine uptake, which can be blocked by AMXT (Fig. 3G). In addition, AMXT could significantly suppresses exogenous polyamine-mediated cell proliferation and viability in ODC cKO, but not WT $CD4^+$ T cells (Fig. 3H and S3C). Similarly, DFMO treatment suppresses human T cell viability and proliferation, which can be restored by polyamine supplement (Fig. S4A and S4B). Importantly, AMXT treatment blocks exogenous polyamine-mediated cell proliferation and viability in human T cells (Fig. S4A and S4B). These results demonstrated that both human and mouse T cells require polyamines for supporting proliferation and survival. In addition, our results suggest that either polyamine biosynthesis or salvage is sufficient to maintain polyamine homeostasis in T cells. Supporting this idea, AMXT treatment alone failed to suppress T cell homeostatic proliferation or antigen-specific proliferation *in vivo* (Fig. S5A

and S5B). These results, together with the results described above, suggest that the salvage pathway and the de novo biosynthesis pathway can compensate for the loss of each other, representing a layer of metabolic plasticity engaged by T cells to maintain polyamine homeostasis.

Simultaneously blocking polyamine salvage and biosynthesis suppresses T cell proliferation *in vivo*

Given that either genetically ablating ODC or pharmacologically blocking polyamine uptake failed to impact T cell proliferation and function *in vivo*, we sought to assess the impacts of simultaneously blocking polyamine salvage and biosynthesis on T cells *in vivo*. We employed competitive homeostatic proliferation and antigen-specific T cell proliferation assays to determine the proliferation of WT and ODC cKO donor $CD4^+$ T cells in recipient mice, which were treated with vehicle or AMXT during the course of experiment. Donor ODC cKO $CD4^+$ T cells recovered from AMXT treated animals but not from vehicle treated animals displayed reduced percentage and delayed proliferation compared with competitive WT $CD4^+$ T cells (Fig. 4A and 4B). We then sought to assess the impacts of simultaneously blocking polyamine salvage and biosynthesis on T cells in the EAE model. The genetic deletion of ODC in T cells failed to cause any significant changes in EAE pathogenic progression. Animals that were treated with AMXT displayed a delayed disease onset initially, but eventually proceeded with pathologic development and reached the endpoint. Importantly, the combination of AMXT with genetic deletion of ODC in T cells conferred full protection against EAE pathogenic progression (Fig. 4C). ODC inhibitor DFMO is an FDA-approved medicine for hirsutism and African sleeping sickness and has been widely tested as a chemopreventive and chemotherapeutic agent

against solid tumors (*30, 31*). Similar to the genetic data, DFMO alone failed to suppress EAE pathogenic progression (Fig. 4D). Although AMXT alone was sufficient to delay EAE onset moderately, it failed to protect animals from reaching the endpoint (Fig. 4D). We envision that the combination of DFMO and AMXT may be sufficient to deplete T cell polyamine pool, and consequently suppress T cell proliferation and effector function *in vivo*. Supporting this idea, the combination of AMXT and DFMO, but not single treatments, conferred full protection against EAE pathogenic progression (Fig. 4D). To evaluate the potential hematological toxicity of DFMO and AMXT combination treatment, we treated CD-1 mice, with AMXT or AMXT plus DFMO at various dose levels for 28 days, and then evaluated a range of hematological parameters at day 29 and at day 43 (after 15 days recovery period). Our results showed that AMXT and DFMO combination treatment does not affect most of hematological parameters (Table. S1). Inflammatory T_H1, T_H17, and FoxP3-expressing regulatory T cells (T_{reg}) are closely related to CD4 T cell subsets but with distinct functions. The balance between pro-inflammatory $CD4^+$ T_{eff} cells and T_{reg} cells determines the pathogenic development of EAE. Next, we examined the polyamine's role in CD4 T_{eff} cell differentiation *in vitro*. Without exogenous polyamine supplemented in cell culture media, maintenance of the intracellular polyamine pool depends solely on ODC-mediated polyamine biosynthesis. Remarkably, intracellular polyamine depletion resulting from ODC deficiency inhibited pro-inflammatory T_H1 and T_H17 cell differentiation while enhancing anti-inflammatory iT_{reg} cell differentiation *in vitro* (Fig. S6A). In EAE animals treated with DFMO in combination with AMXT, we observed a significant reduction of $CD4^+$ T cell infiltration into the central nervous system (CNS) and a reduction of $IL17^+$ $CD4^+$ T cell in CNS comparing to control group (Fig. S6B). Together, our results indicate that the polyamine blocking approach, via ablation of salvage and biosynthesis pathways,

suppresses T cell proliferation and inflammatory functions, and may be a potential new therapy for treating inflammatory and autoimmune disease.

Amino acid catabolism provides carbon sources for polyamine biosynthesis

Dietary intake and intestinal microbiota metabolism are major sources of circulating polyamine (*27*). We reasoned that an understanding of carbon sources that drive polyamine biosynthesis in T cells would enable the development of nutritional approaches for effectively controlling polyamine homeostasis in T cells. While arginine catabolism is integrated into the urea cycle to detoxify ammonia and provides the precursor for polyamine biosynthesis, we previously reported that glutamine-derived carbon could be funneled into polyamine biosynthesis through ornithine in T cells (*13*). In addition, proline can also provide carbon for polyamine biosynthesis in the placenta and in plants (*32*). To determine to what extent these three amino acids contribute to polyamine biosynthesis, we applied the stable isotope of carbon-13 (^{13}C) labeling and mass spectrometry approach. We supplied $^{13}C_6$-Arginine, $^{13}C_5$-Glutamine, or $^{13}C_5$-Proline as metabolic tracers in T cell culture media and then followed ^{13}C incorporation into individual metabolites (Fig. 5A). While not all selected metabolites were detected in our experiment due to technical limitation and a portion of proline was produced through de novo biosynthesis, our results clearly demonstrated that $^{13}C_5$-Proline only contributes a minimal amount of $^{13}C_5$ isotopologue of ornithine and polyamine (Fig. 5B). In contrast, $^{13}C_6$-Arginine and $^{13}C_5$-Glutamine contribute 50% and 40% of $^{13}C_5$-Ornithine, respectively (Fig. 5B). Importantly, $^{13}C_6$-Arginine and $^{13}C_5$-Glutamine contribute around 80% and 20% of $^{13}C_4$ isotopologues of polyamine (putrescine and spermidine generated via decarboxylation of ornithine), respectively (Fig. 5B). Thus, we

conclude that arginine is a major carbon donor and glutamine is a minor carbon donor for supporting polyamine biosynthesis in T cells *in vitro*.

Arginine catabolism drives T cell proliferation partially through supporting polyamine biosynthesis

While arginine is generally considered a non-essential amino acid, T cells are arginine auxotrophic *in vitro* (*18*). Arginine is required to maintain $CD4^+$ T cells viability, driving proliferative and proinflammatory lineage (T_H17) differentiation (Fig. 5C-E). While the amount of most amino acids is in the low micromolar (μM) range, the concentration of arginine is in the millimolar (mM) range in cell culture media. We envisioned that, in addition to a general requirement of arginine for protein synthesis, arginine might also support T cell proliferation and differentiation through polyamine biosynthesis. To test this idea, we titrated down the amount of arginine in cell culture media and found that 10 μM of arginine was sufficient to support protein synthesis and the growth of cell mass at the early time point after T cell activation but failed to maintain cell viability and drive proliferation later (Fig. S7A and S7B). We envision that arginine supports protein synthesis and polyamine biosynthesis, both of which are required to drive T cell proliferation. Supporting this idea, we have shown that a low level of arginine (10 μM) in culture media is sufficient to support protein synthesis, but not proliferation (Fig. S7A). Similar to what we found in arginine depletion condition, low level of arginine (10 μM, with or without daily replenishment) in culture media failed to support T cell proliferation and an optimal T_H17 differentiation (Fig. S8B and S8C). However, polyamine supplements can partially restore T cell proliferation and T_H17 differentiation with a low level of arginine (10 μM, with or without daily replenishment) (Fig. S8B and S8C). In contrast,

polyamine supplements failed to restore T cell proliferation and differentiation under arginine starvation condition (0 μM) (Fig. S8A). Collectively, our data indicate that T cell activation engages a metabolic axis that connects arginine catabolism to polyamine de novo biosynthesis.

Discussion

Fast-growing pathogens impose selective pressures on the metabolic fitness and metabolic plasticity of host immune cells, which are necessary for immune cells to maintain homeostasis while remaining ready to mount rapid responses under diverse metabolic and immune conditions (*24, 33-36*). A robust T cell-mediated adaptive immune response exhibits high and dynamic metabolic demands in T cells, which is accommodated through fine-tuned regulation on both the central carbon metabolic pathways, and peripheral metabolic pathways including polyamine metabolism (*4, 5, 9, 19*). The standard formulation of cell culture media, which does not fully recapitulate the physiological metabolite composition in the plasma and tissue microenvironment, often leads to a significant metabolic adaptation of growing cells *in vitro*. Metabolic phenotypes of cells growing *in vivo* may further differ from cells growing *in vitro* as a result of other environmental factors including oxygen level, cellular competition and cooperation, and the biophysical properties of the extracellular matrix (*37-39*). Similarly, T cell metabolism can respond and adapt to environmental nutrient levels (*24, 40*). Our studies revealed T cells' capacity to engage in both de novo biosynthetic and salvage pathways to fine-tune polyamine homeostasis, which is required to maximize metabolic fitness and optimize CD4 T_{eff} cell proliferation and differentiation. Such metabolic plasticity is likely to be crucial for T cells' ability to elicit robust immune responses in different tissue contexts.

Glutamine and arginine are two non-essential amino acids that not only fulfill the general requirements for protein synthesis, but also connect central carbon metabolism to a variety of biosynthetic pathways to produce specialized metabolites (*41-44*). Glutamine catabolism funnels the anaplerotic flux of carbon into the TCA cycle and also provides sources of nitrogen and carbon to support biosynthesis of nonessential amino acids, lipids, nucleotides, glutathione and polyamines in T cells (*13, 45, 46*). Similarly, arginine is critical for maintaining T cells viability, driving proliferative and effector functions (*14*). We found that polyamine supplement could partially relieve T cell's dependence on arginine, indicating that a key role of arginine catabolism in T cells is to support polyamine biosynthesis. Consistently, arginine serves as a major donor of carbon in polyamine biosynthesis, while glutamine only plays a minor role in funneling carbon into polyamine in the presence of arginine in vitro. Interestingly, these two amino acids contribute a comparable portion of carbon to ornithine, the precursor of polyamine. This finding is in line with previous studies showing that arginine-derived ornithine is not the only source for endogenous ornithine in most mammalian tissues (*47*). In addition, our findings may implicate ornithine as an important metabolic node representing a key branch point in both glutamine and arginine catabolic pathways. Ornithine can be committed towards the urea cycle, proline biosynthesis or de novo synthesis of polyamine. The production of ornithine from two different metabolic precursors, glutamine and arginine, also enables fine-tuned coordination between the metabolic flux shunted towards polyamine synthesis and the metabolic flux shunted towards other specialized metabolites. Consistent with this idea, the overall high consumption rate of glutamine and arginine may provide a sensitive and precise regulation on intermediate metabolites that can be committed toward several metabolic branches, hence permitting rapid responses to meet the metabolic demands of cell growth and cytokine production.

Active T cells and other highly proliferative cells such as tumor cells share metabolic characteristics and are strictly dependent on the catabolism of glucose and glutamine through the central carbon metabolic pathways (*48*). Similarly, elevated levels of polyamine are associated with T cell activation and cell transformation (*13*, *49*). Importantly, pharmacologic or genetic targeting of ODC, a transcriptional target of proto-oncogene MYC, could delay the development and the progression of MYC-driven tumors in mice (*50*). While pharmacologic agents targeting polyamines such as the ODC inhibitor DFMO has generally low toxicity, DFMO yields only very marginal therapeutic benefits in cancer patients as a single-agent therapy in clinical trials (*51*). Clearly, cancer cells are capable of importing polyamine from circulation to overcome the effect of DFMO. Supporting this idea, the simultaneous blockage of polyamine biosynthesis and uptake has generated promising results in tumor preclinical animal models (*29*). Mammalian cells can uptake polyamine through endocytosis and membrane transport system mediated by several solute carrier transporters (*52*). AMXT 1501 is a novel lipophilic polyamine mimetic that potently blocks polyamine uptake through competing with polyamine (*28*). The combination of AMXT 1501 and DFMO could effectively deplete the polyamine pool in tumor cells and suppress the growth of tumors in various animal models (*29*). These promising preclinical studies led to a recently opened Phase I clinical trial in solid tumors (NCT03077477). Similarly, we have shown that ODC cKO $CD4^+$ T cells proliferate and function normal *in vivo*. However, concurrent treatment of ODC cKO $CD4^+$ T cells with AMXT 1501 abrogate their proliferation and inflammatory function *in vivo*. Moreover, the combination of AMXT 1501 and DFMO could confer full protection to mice against pathogenic development of EAE. Thus, polyamine

blocking strategy via simultaneous blockade of polyamine biosynthesis and salvage may present a promising and novel therapy for treating inflammatory and autoimmune diseases.

Materials and Methods

Mice

C57BL/6 (WT) mice, *Rag1*$^{-/-}$ mice (B6.129S7-*Rag1*^{tm1Mom}/J), OT-II mice (B6.Cg-Tg(TcraTcrb)425Cbn/J), Thy1.1^{+} mice (B6.PL-*Thy1*^{a}/CyJ), and CD45.1^{+} mice (B6.SJL-*Ptprc*^{a} *Pepc*^{b}/BoyJ) were obtained from the Jackson Laboratory (JAX, Bar Harbor, ME). Mice with one targeted allele of ODC on the C57BL/6 background (Odc1$^{tm1a(EUCOMM)Hmgu/J}$) were generated by the Knockout Mouse Phenotyping Program (KOMP^{2}) at the JAX. The mice were first crossed with a transgenic Flippase strain (B6.129S4-*Gt(ROSA)26Sor*$^{tm1(FLP1)Dym}$/RainJ) to remove the LacZ-reporter allele, and then crossed with the CD4-Cre strain to generate T cell-specific ODC knockout strain (ODC cKO). Gender and age matched mice (6-12 weeks old) were used for all the experiments. All mice were maintained in specific pathogen-free conditions at the Nationwide Children Hospital animal facility and all the animal studies were approved by the Institutional Animal Care and Use Committee of the Abigail Wexner Research Institute at Nationwide Children's Hospital (IACUC; protocol number AR13-00055).

Flow cytometry

For analysis of surface markers, cells were stained in phosphate-buffered saline (PBS) containing 2% (w/v) bovine serum albumin (BSA) and the appropriate antibodies from Biolegend for 30

min at 4°C. For intracellular cytokine staining, cells were stimulated for 4 hours with Cell Stimulation Cocktails of phorbol 12-myristate 13-acetate (PMA), ionomycin, brefieldin A and monensin (eBioscience). Cells were then washed with PBS, fixed and permeabilized using FoxP3 Fixation/Permeabilization Kit according to the manufacturer's instructions (eBioscience). Cells were then stained with anti-IFN-γ and anti-IL-17A antibodies (Biolegend); For intracellular FoxP3 staining, cells were fixed, permeabilized, and stained with anti-FoxP3 antibody (Biolegend). For protein content measurement, cells were fixed with 4% para-formaldehyde for 30 min at 4°C, permeabilized with FoxP3 permeabilization solution (eBioscience), and then stained with FITC (Fisher scientific). For CFSE staining, freshly isolated T cells were incubated with 4 μM CFSE (Invitrogen) in PBS at room temperature for 10 min, then washed three times with cell culture medium containing 10% FBS. For cell viability analysis, cells were stained with 7AAD (Biolegend) for 5 min before running on a flow cytometer. All flow cytometry data were acquired on Novocyte (ACEA Biosciences) and were analyzed with FlowJo software (BD Biosciences).

Cell Culture

Human peripheral blood mononuclear cells (PBMCs) were isolated from buffy coat (American Red Cross) using Ficoll/Hypaque density gradient centrifugation. Human $CD4^+$ naïve T cells were directly enriched from PBMCs using human CD4 naïve T cell Isolation Kit (MojoSort, Biolegend) following the manufacturer's instructions. Isolated human T cells (1×10^6 cells/mL) were stimulated with plate-bound anti-hCD3 and anti-hCD28 antibodies and cultured in RPMI-1640 medium (Gibco, Thermo Fisher Scientific) supplemented with 10% (v/v) heat-inactivated dialyzed fetal bovine serum (DFBS), 2 mM L-glutamine, 1% sodium pyruvate (Sigma-Aldrich), 100 units/mL penicillin, and 100 μg/mL streptomycin, in the present of hIL-2 (100 U/mL, Bio X

Cell) at 37°C/5% CO_2. Culture plates were pre-coated with 1 μg/mL anti-hCD3 and 1 μg/mL anti-hCD28 antibodies (Bio X Cell) overnight at 4°C. DFBS was made by dialyzing against 100 volumes of PBS (five changes in three days) using Slide-ALyzerTM G2 dialysis cassettes with cut-through MW size 2K (ThermoFisher Scientific) at 4°C to remove any potential polyamines in the FBS (Atlanta Biologicals).

Total $CD3^+$ T cells or naïve $CD4^+$ T cells were isolated from mouse spleen and lymph nodes using murine CD3 or CD4 naïve T cell Isolation Kit (MojoSort, Biolegend) following the manufacturer's instructions. Freshly isolated mouse T cells (1×10^6 cells/mL) were either maintained in culture media containing 5 ng/mL mouse IL-7 or were stimulated with mouse IL-2 (100 U/mL) as well as plate-bound anti-mCD3 and anti-mCD28 antibodies, and cultured with the medium described above with 0.05 mM 2-mercaptoethanol (Sigma-Aldrich). Culture plates were pre-coated with 2 μg/mL anti-mCD3 (clone 145-2C11, Bio X Cell) and 2 μg/mL anti-mCD28 (clone 37.51, Bio X Cell) antibodies overnight at 4°C. For CD4 T cell polarization, freshly isolated naïve $CD4^+$ T cells (0.6×10^6/mL) were stimulated with cytokine and neutralizing antibody cocktail as well as plate-bound anti-mCD3 and anti-mCD28 antibodies. Specifically, culture plates were pre-coated with 5 μg/mL(for iT_{reg} and T_H1) or 10 μg/mL(for T_H17) anti-mCD3 and anti-mCD28 antibodies overnight at 4°C. Cytokines and neutralizing antibody cocktails include mIL-2 (200 U/mL) and hTGF-β1 (5 ng/mL, PeproTech) for iT_{reg} differentiation; mIL-6 (50 ng/mL, PeproTech), hTGF-β1 (2 ng/mL), anti–mIL-2 (8 μg/mL, Bio X Cell), anti–mIL-4 (8 μg/mL, Bio X Cell), and anti–mIFN-γ (8 μg/mL, Bio X Cell) for T_H17 differentiation; and mIL-2 (200 U/mL), mIL-12 (5 ng/mL, PeproTech), and anti–mIL-4 (10 μg/mL) for T_H1 differentiation. DFMO (2 mM, Carbosynth) and AMXT 1501 (1 μM, Aminex Therapeutics) were added into the cell culture medium in the indicated experiments. For

polyamine supplementation experiment, polyamine mixture including putrescine, spermidine, and spermine (1µM, Sigma-Aldrich) was added into culture medium along with aminoguanidine (0.2 mM, Sigma-Aldrich), which inhibits diamine oxidase in the FBS.

Cell cycle analysis

T cell cycle analysis was performed using Phase-Flow Alexa Fluro 647 BrdU Kit (Biolegend) per the manufacturer's instructions. Briefly, T cells were pulsed with 10 µg/mL BrdU for 1 hr followed by surface staining, fixation, and permeabilization. BrdU incorporated into the DNA during S phase were recognized by intracellular BrdU antibody staining, and total DNA content was used to differentiate G1 and G2 stages by 7AAD labeling.

qPCR

Total RNA was isolated using the RNeasy Mini Kit (Qiagen) and was reverse transcribed using random hexamers and M-MLV Reverse Transcriptase (Invitrogen). SYBR green-based quantitative RT-PCR was performed using the BIO-RAD CFX96^{TM} Real-Time PCR Detection System. The relative gene expression was determined by the comparative *CT* method, also referred to as the $2^{-\Delta\Delta CT}$ method. The data were presented as the fold change in gene expression normalized to an internal reference gene (beta2-microglobulin) and relative to the control (the first sample in the group). Fold change = $2^{-\Delta\Delta C_T}$ = [($CT_{\text{gene of interest}}$- $CT_{\text{internal reference}}$)] sample A - [($CT_{\text{gene of interest}}$- $CT_{\text{internal reference}}$)] sample B. Samples for each experimental condition were run in triplicated PCR reactions. ODC1 primer sequences (Forward: GCATGCATCTGCTTGATATTGG and Reverse: GTCCAGAGCTGGGTTGATTAC) were obtained from PrimerBank.

Putrescine uptake assay

2 $\times 10^6$ T cells were suspended in 200 uL PBS containing permeant putrescine (100 μM) and [1,4-^{14}C]-putrescine dihydrochloride (0.2 uCi, ARC 0245) then incubated at 37°C for 10 min (within the established linear phase of uptake). The uptake was stopped by loading all the transport mixture onto a discontinuous gradient of bromododecane and perchloric acid/sucrose then centrifuged at 14, 000 ×*g* for 90 sec. The discontinuous gradient was prepared by overlaying 1-Bromododecane (800 μL, Sigma-Aldrich) above 20% perchloric acid (100 μL, Sigma-Aldrich)/8% sucrose solution in 1.5 mL microfuge tube. The samples were snap-frozen in an ethanol-dry ice bath. The bottom part of microfuge tubes containing T cell lysate in perchloric acid-sucrose was cut by a microfuge cutter. The cell lysates were diluted with 300 μL of 0.5% SDS-1% TritonX100, and then transferred into scintillation vials with 10 mL scintillation cocktail. The radioactivity was quantitated by liquid scintillation spectrometry.

Adoptive cell transfer and *in vivo* proliferation

For homeostatic proliferation assay, naïve CD4$^+$ T cells isolated from WT(Thy1.1$^+$) and ODC cKO(Thy1.2$^+$) donor mice were labeled with CFSE as described above, and then were mixed with 1:1 ratio. Approximately 1 $\times 10^7$ mixed cells in 150 μL PBS were injected via retro-orbital venous sinus into gender-matched *Rag1*$^{-/-}$ mice, which were sacrificed 4 days later. Lymph nodes were collected and cell proliferation was assessed by flow cytometry analysis.

For Ova-antigen driven proliferation assay, naïve CD4$^+$ T cells isolated from OT-II-WT (Thy1.1$^+$) and OT-II-ODC cKO(Thy1.2$^+$) donor mice were labeled with CFSE as described above, and then were mixed with 1:1 ratio. Approximately 1 $\times 10^7$ mixed cells in 150 μL PBS were injected via retro-orbital venous sinus into gender-matched CD45.1$^+$ mice. One day after cell injection, host mice were immunized subcutaneously in the hock area of both legs with 50

μL OVA$^{323-339}$ peptide (1 mg/mL, InvivoGen) emulsified with complete freund adjuvant (CFA, InvivoGen). Seven days after immunization, lymph organs of host mice were collected for cell surface staining and flow cytometry analysis.

Experimental Autoimmune Encephalomyelitis (EAE) Induction and Assessment

Mice were immunized subcutaneously with 100 μg of myelin oligodendrocyte glycoprotein $(MOG)_{35–55}$ peptide emulsified in CFA (mixture of IFA (Difco) and mycobacterium tuberculosis (Difco)). Mice were intraperitoneal (i.p) injected with 200 ng of pertussis toxin (PTX, List Biological Laboratories) on the day of immunization and 2 days later. For the DFMO treated group, mice were fed with 1% DFMO in drinking water which was replenished every five days throughout the experiment. For the AMXT 1501 treated group, mice received 3 mg/kg of AMXT 1501 subcutaneous daily throughout the experiment. All mice were observed daily for clinical signs and scored as described below.

Score 1	Limp tail. When the mouse is picked up by the tail, the whole tail drapes over your finger, instead of being erect.
Score 2	Limp tail and weakness of hind legs. When mouse is picked up by tail, legs are not spread apart, but held closer together. When the mouse is observed when walking, it has a clearly apparent wobbly walk.
Score 3	Limp tail and complete paralysis of hind legs (most common). OR Limp tail with paralysis of one front and one hind legs.
Score 4	Limp tail, complete hind leg and partial front leg paralysis. Mouse is minimally moving around the cage but appears alert and feeding. Usually, euthanasia is recommended

In some experiment, mice were sacrificed when control mice reached the onset of symptom or when control mice reached terminal end-stage as indicated. The central nervous system (CNS) (brain and spinal cord), spleen, and peripheral lymph nodes (PLN) were collected, and then single cell suspension of each organ were prepared. To isolate mononuclear cells from CNS, cell suspension was centrifuged on a 30%/70% percoll gradient at 500 ×*g* for 30 min. Isolated cells were activated for 4 hr using cell stimulation cocktail, surface staining and intracellular staining were performed prior to flow cytometric analysis. as described above.

CE-QqQ/TOFMS analysis

$CD3^+$ T cells (around 1.5×10^7 cells/sample) isolated from WT or ODC cKO mice were activated for 36 hr and then used for the extraction of intracellular metabolites. The cells were collected by centrifugation (300 ×*g* at 4ºC for 5 min) and washed twice with 5% mannitol solution (10 mL first and then 2 mL), then treated with 800 µL of methanol and vortexed for 30 sec in order to inactivate enzymes. Next, the cell extract was treated with 550 µL of Milli-Q water containing internal standards (H3304-1002, Human Metabolome Technologies, inc., Tsuruoka, Japan) and vortexed for 30 sec. The extract was obtained and centrifuged at 2,300 ×*g* and 4ºC for 5 min, and then 700 µL of upper aqueous layer was centrifugally filtered through a Millipore 5-kDa cutoff filter at 9,100 ×*g* and 4ºC for 180 min to remove proteins. The filtrate was centrifugally concentrated and re-suspended in 50 µL of Milli-Q water for CE-MS analysis. Cationic compounds were measured in the positive mode of CE-TOFMS and anionic compounds were measured in the positive and negative modes of CE-MS/MS. Peaks detected by CE-TOFMS and CE-MS/MS were extracted using an automatic integration software (MasterHands, Keio University, Tsuruoka, Japan and MassHunter Quantitative Analysis B.04.00, Agilent

Technologies, Santa Clara, CA, USA, respectively) in order to obtain peak information including *m/z*, migration time (MT), and peak area. The peaks were annotated with putative metabolites from the HMT metabolite database based on their MTs in CE and *m/z* values determined by TOFMS. The tolerance range for the peak annotation was configured at ±0.5 min for MT and ±10 ppm for *m/z*. In addition, concentrations of metabolites were calculated by normalizing the peak area of each metabolite with respect to the area of the internal standard and by using standard curves, which were obtained by three-point calibrations.

Hierarchical cluster analysis (HCA) and principal component analysis (PCA) were performed by our proprietary software, PeakStat and SampleStat, respectively. Detected metabolites were plotted on metabolic pathway maps using VANTED (Visualization and Analysis of Networks containing Experimental Data) software.

CE-TOFMS analysis

$CD3^+$ T cells (around 1.8×10^7 cells/sample) were activated for 36 hours in conditional media (RPMI-1640) containing 2 mM $^{13}C_5$-Glutamine, 1.15 mM $^{13}C_6$-Arginine, or 0.17 mM $^{13}C_5$-Proline, and then used for the extraction of intracellular metabolites as described above. Metabolome measurements were carried out through a facility service at Human Metabolome Technology Inc., Tsuruoka, Japan. CE-TOFMS measurement was carried out using an Agilent CE Capillary Electrophoresis System equipped with an Agilent 6210 Time of Flight mass spectrometer, Agilent 1100 isocratic HPLC pump, Agilent G1603A CE-MS adapter kit, and Agilent G1607A CE-ESI-MS sprayer kit (Agilent Technologies, Waldbronn, Germany). The systems were controlled by Agilent G2201AA ChemStation software version B.03.01 for CE (Agilent Technologies, Waldbronn, Germany). The metabolites were analyzed by using a fused silica capillary (50 μm *i.d.* × 80 cm total length), with commercial electrophoresis buffer

(Solution ID: H3301-1001 for cation analysis and H3302-1021 for anion analysis, Human Metabolome Technologies) as the electrolyte. The sample was injected at a pressure of 50 mbar for 10 sec (approximately 10 nL) in cation analysis and 25 sec (approximately 25 nL) in anion analysis. The spectrometer was scanned from *m/z* 50 to 1,000.

Statistical analysis

Statistical analysis was conducted using the GraphPad Prism software (GraphPad Software, Inc.). *P* values were calculated with two-way ANOVA for the EAE experiments. Unpaired two tail student's t-test, multiple comparisons of one/ two-way ANOVA or Dunnett LSD test was used to assess differences in other experiments. *P* values smaller than 0.05 were considered significant, with $p < 0.05$, $p < 0.01$, $p < 0.001$, and $p < 0.0001$ indicated as *, **, ***, and ****, respectively.

References

1. D. Finlay, D. A. Cantrell, Metabolism, migration and memory in cytotoxic T cells. *Nature reviews. Immunology* **11**, 109-117 (2011).
2. R. Wang, D. R. Green, Metabolic reprogramming and metabolic dependency in T cells. *Immunol Rev* **249**, 14-26 (2012).
3. S. E. Weinberg, L. A. Sena, N. S. Chandel, Mitochondria in the regulation of innate and adaptive immunity. *Immunity* **42**, 406-417 (2015).
4. L. A. O'Neill, R. J. Kishton, J. Rathmell, A guide to immunometabolism for immunologists. *Nature reviews. Immunology* **16**, 553-565 (2016).
5. E. L. Pearce, M. C. Poffenberger, C. H. Chang, R. G. Jones, Fueling immunity: insights into metabolism and lymphocyte function. *Science* **342**, 1242454 (2013).

6. R. F. Bertolo, D. G. Burrin, Comparative aspects of tissue glutamine and proline metabolism. *J Nutr* **138**, 2032S-2039S (2008).

7. G. Wu, A. G. Borbolla, D. A. Knabe, The uptake of glutamine and release of arginine, citrulline and proline by the small intestine of developing pigs. *J Nutr* **124**, 2437-2444 (1994).

8. R. Majumdar, B. Barchi, S. A. Turlapati, M. Gagne, R. Minocha, S. Long, S. C. Minocha, Glutamate, Ornithine, Arginine, Proline, and Polyamine Metabolic Interactions: The Pathway Is Regulated at the Post-Transcriptional Level. *Front Plant Sci* **7**, 78 (2016).

9. D. J. Puleston, M. Villa, E. L. Pearce, Ancillary Activity: Beyond Core Metabolism in Immune Cells. *Cell Metab* **26**, 131-141 (2017).

10. A. E. Pegg, Functions of Polyamines in Mammals. *J Biol Chem* **291**, 14904-14912 (2016).

11. V. Bronte, P. Zanovello, Regulation of immune responses by L-arginine metabolism. *Nature reviews. Immunology* **5**, 641-654 (2005).

12. L. Miller-Fleming, V. Olin-Sandoval, K. Campbell, M. Ralser, Remaining Mysteries of Molecular Biology: The Role of Polyamines in the Cell. *J Mol Biol* **427**, 3389-3406 (2015).

13. R. Wang, C. P. Dillon, L. Z. Shi, S. Milasta, R. Carter, D. Finkelstein, L. L. McCormick, P. Fitzgerald, H. Chi, J. Munger, The transcription factor Myc controls metabolic reprogramming upon T lymphocyte activation. *Immunity* **35**, 871-882 (2011).

14. R. Geiger, J. C. Rieckmann, T. Wolf, C. Basso, Y. Feng, T. Fuhrer, M. Kogadeeva, P. Picotti, F. Meissner, M. Mann, N. Zamboni, F. Sallusto, A. Lanzavecchia, L-Arginine

Modulates T Cell Metabolism and Enhances Survival and Anti-tumor Activity. *Cell* **167**, 829-842 e813 (2016).

15. D. M. Hardbower, M. Asim, P. B. Luis, K. Singh, D. P. Barry, C. Yang, M. A. Steeves, J. L. Cleveland, C. Schneider, M. B. Piazuelo, A. P. Gobert, K. T. Wilson, Ornithine decarboxylase regulates M1 macrophage activation and mucosal inflammation via histone modifications. *Proc Natl Acad Sci U S A* **114**, E751-E760 (2017).

16. H. Zhang, G. Alsaleh, J. Feltham, Y. Sun, G. Napolitano, T. Riffelmacher, P. Charles, L. Frau, P. Hublitz, Z. Yu, S. Mohammed, A. Ballabio, S. Balabanov, J. Mellor, A. K. Simon, Polyamines Control eIF5A Hypusination, TFEB Translation, and Autophagy to Reverse B Cell Senescence. *Mol Cell* **76**, 110-125 e119 (2019).

17. D. J. Puleston, M. D. Buck, R. I. Klein Geltink, R. L. Kyle, G. Caputa, D. O'Sullivan, A. M. Cameron, A. Castoldi, Y. Musa, A. M. Kabat, Y. Zhang, L. J. Flachsmann, C. S. Field, A. E. Patterson, S. Scherer, F. Alfei, F. Baixauli, S. K. Austin, B. Kelly, M. Matsushita, J. D. Curtis, K. M. Grzes, M. Villa, M. Corrado, D. E. Sanin, J. Qiu, N. Pallman, K. Paz, M. E. Maccari, B. R. Blazar, G. Mittler, J. M. Buescher, D. Zehn, S. Rospert, E. J. Pearce, S. Balabanov, E. L. Pearce, Polyamines and eIF5A Hypusination Modulate Mitochondrial Respiration and Macrophage Activation. *Cell Metab* **30**, 352-363 e358 (2019).

18. P. J. Murray, Amino acid auxotrophy as a system of immunological control nodes. *Nat Immunol* **17**, 132-139 (2016).

19. R. Wang, D. R. Green, Metabolic checkpoints in activated T cells. *Nat Immunol* **13**, 907-915 (2012).

20. H. Zeng, H. Chi, mTOR signaling in the differentiation and function of regulatory and effector T cells. *Current opinion in immunology* **46**, 103-111 (2017).

21. J. N. R. Gnanaprakasam, J. W. Sherman, R. Wang, MYC and HIF in shaping immune response and immune metabolism. *Cytokine Growth Factor Rev* **35**, 63-70 (2017).

22. J. D. Powell, G. M. Delgoffe, The mammalian target of rapamycin: linking T cell differentiation, function, and metabolism. *Immunity* **33**, 301-311 (2010).

23. L. Z. Shi, R. Wang, G. Huang, P. Vogel, G. Neale, D. R. Green, H. Chi, HIF1alpha-dependent glycolytic pathway orchestrates a metabolic checkpoint for the differentiation of TH17 and Treg cells. *J Exp Med* **208**, 1367-1376 (2011).

24. M. Slack, T. Wang, R. Wang, T cell metabolic reprogramming and plasticity. *Molecular immunology* **68**, 507-512 (2015).

25. H. Pendeville, N. Carpino, J. C. Marine, Y. Takahashi, M. Muller, J. A. Martial, J. L. Cleveland, The ornithine decarboxylase gene is essential for cell survival during early murine development. *Mol Cell Biol* **21**, 6549-6558 (2001).

26. W. C. Skarnes, B. Rosen, A. P. West, M. Koutsourakis, W. Bushell, V. Iyer, A. O. Mujica, M. Thomas, J. Harrow, T. Cox, D. Jackson, J. Severin, P. Biggs, J. Fu, M. Nefedov, P. J. de Jong, A. F. Stewart, A. Bradley, A conditional knockout resource for the genome-wide study of mouse gene function. *Nature* **474**, 337-342 (2011).

27. E. Larque, M. Sabater-Molina, S. Zamora, Biological significance of dietary polyamines. *Nutrition* **23**, 87-95 (2007).

28. M. R. Burns, G. F. Graminski, R. S. Weeks, Y. Chen, T. G. O'Brien, Lipophilic lysine-spermine conjugates are potent polyamine transport inhibitors for use in combination with a polyamine biosynthesis inhibitor. *J Med Chem* **52**, 1983-1993 (2009).

29. L. D. Gamble, S. Purgato, J. Murray, L. Xiao, D. M. T. Yu, K. M. Hanssen, F. M. Giorgi, D. R. Carter, A. J. Gifford, E. Valli, G. Milazzo, A. Kamili, C. Mayoh, B. Liu, G. Eden, S. Sarraf, S. Allan, S. Di Giacomo, C. L. Flemming, A. J. Russell, B. B. Cheung, A. Oberthuer, W. B. London, M. Fischer, T. N. Trahair, J. I. Fletcher, G. M. Marshall, D. S. Ziegler, M. D. Hogarty, M. R. Burns, G. Perini, M. D. Norris, M. Haber, Inhibition of polyamine synthesis and uptake reduces tumor progression and prolongs survival in mouse models of neuroblastoma. *Sci Transl Med* **11**, (2019).

30. P. G. Kennedy, Clinical features, diagnosis, and treatment of human African trypanosomiasis (sleeping sickness). *Lancet Neurol* **12**, 186-194 (2013).

31. A. C. Vissing, E. H. Taudorf, C. S. Haak, P. A. Philipsen, M. Haedersdal, Adjuvant eflornithine to maintain IPL-induced hair reduction in women with facial hirsutism: a randomized controlled trial. *J Eur Acad Dermatol Venereol* **30**, 314-319 (2016).

32. G. Wu, F. W. Bazer, J. Hu, G. A. Johnson, T. E. Spencer, Polyamine synthesis from proline in the developing porcine placenta. *Biol Reprod* **72**, 842-850 (2005).

33. S. Weis, A. R. Carlos, M. R. Moita, S. Singh, B. Blankenhaus, S. Cardoso, R. Larsen, S. Rebelo, S. Schauble, L. Del Barrio, G. Mithieux, F. Rajas, S. Lindig, M. Bauer, M. P. Soares, Metabolic Adaptation Establishes Disease Tolerance to Sepsis. *Cell* **169**, 1263-1275 e1214 (2017).

34. E. D. Weinberg, Nutritional immunity. Host's attempt to withold iron from microbial invaders. *JAMA* **231**, 39-41 (1975).

35. Y. Abu Kwaik, D. Bumann, Microbial quest for food in vivo: 'nutritional virulence' as an emerging paradigm. *Cell Microbiol* **15**, 882-890 (2013).

36. K. Troha, J. S. Ayres, Metabolic Adaptations to Infections at the Organismal Level. *Trends Immunol* **41**, 113-125 (2020).

37. M. R. Sullivan, L. V. Danai, C. A. Lewis, S. H. Chan, D. Y. Gui, T. Kunchok, E. A. Dennstedt, M. G. Vander Heiden, A. Muir, Quantification of microenvironmental metabolites in murine cancers reveals determinants of tumor nutrient availability. *Elife* **8**, (2019).

38. J. R. Cantor, The Rise of Physiologic Media. *Trends Cell Biol* **29**, 854-861 (2019).

39. T. Ackermann, S. Tardito, Cell Culture Medium Formulation and Its Implications in Cancer Metabolism. *Trends Cancer* **5**, 329-332 (2019).

40. E. H. Ma, M. J. Verway, R. M. Johnson, D. G. Roy, M. Steadman, S. Hayes, K. S. Williams, R. D. Sheldon, B. Samborska, P. A. Kosinski, H. Kim, T. Griss, B. Faubert, S. A. Condotta, C. M. Krawczyk, R. J. DeBerardinis, K. M. Stewart, M. J. Richer, V. Chubukov, T. P. Roddy, R. G. Jones, Metabolic Profiling Using Stable Isotope Tracing Reveals Distinct Patterns of Glucose Utilization by Physiologically Activated CD8(+) T Cells. *Immunity* **51**, 856-870 e855 (2019).

41. E. Kvamme, G. Svenneby, Effect of anaerobiosis and addition of keto acids on glutamine utilization by Ehrlich ascites-tumor cells. *Biochim Biophys Acta* **42**, 187-188 (1960).

42. R. J. DeBerardinis, J. J. Lum, G. Hatzivassiliou, C. B. Thompson, The biology of cancer: metabolic reprogramming fuels cell growth and proliferation. *Cell Metab* **7**, 11-20 (2008).

43. B. J. Altman, Z. E. Stine, C. V. Dang, From Krebs to clinic: glutamine metabolism to cancer therapy. *Nat Rev Cancer* **16**, 619-634 (2016).

44. S. M. Morris, Jr., Arginine metabolism: boundaries of our knowledge. *J Nutr* **137**, 1602S-1609S (2007).

45. G. Lian, J. R. Gnanaprakasam, T. Wang, R. Wu, X. Chen, L. Liu, Y. Shen, M. Yang, J. Yang, Y. Chen, V. Vasiliou, T. A. Cassel, D. R. Green, Y. Liu, T. W. Fan, R. Wang, Glutathione de novo synthesis but not recycling process coordinates with glutamine catabolism to control redox homeostasis and directs murine T cell differentiation. *Elife* **7**, (2018).

46. D. Klysz, X. Tai, P. A. Robert, M. Craveiro, G. Cretenet, L. Oburoglu, C. Mongellaz, S. Floess, V. Fritz, M. I. Matias, C. Yong, N. Surh, J. C. Marie, J. Huehn, V. Zimmermann, S. Kinet, V. Dardalhon, N. Taylor, Glutamine-dependent alpha-ketoglutarate production regulates the balance between T helper 1 cell and regulatory T cell generation. *Sci Signal* **8**, ra97 (2015).

47. J. L. Deignan, J. C. Livesay, P. K. Yoo, S. I. Goodman, W. E. O'Brien, R. K. Iyer, S. D. Cederbaum, W. W. Grody, Ornithine deficiency in the arginase double knockout mouse. *Mol Genet Metab* **89**, 87-96 (2006).

48. T. Wang, G. Liu, R. Wang, The Intercellular Metabolic Interplay between Tumor and Immune Cells. *Front Immunol* **5**, 358 (2014).

49. E. W. Gerner, F. L. Meyskens, Jr., Polyamines and cancer: old molecules, new understanding. *Nat Rev Cancer* **4**, 781-792 (2004).

50. C. Bello-Fernandez, G. Packham, J. L. Cleveland, The ornithine decarboxylase gene is a transcriptional target of c-Myc. *Proc Natl Acad Sci U S A* **90**, 7804-7808 (1993).

51. R. A. Casero, Jr., T. Murray Stewart, A. E. Pegg, Polyamine metabolism and cancer: treatments, challenges and opportunities. *Nat Rev Cancer* **18**, 681-695 (2018).

52. A. A. Abdulhussein, H. M. Wallace, Polyamines and membrane transporters. *Amino Acids* **46**, 655-660 (2014).

Acknowledgments

General: We thank John Sherman and Hayley Rodgers for critically reading and editing the manuscript.

Funding: This work was supported by 1R21CA227926-01A1 and 1UO1CA232488-01 from National Institute of Health (Cancer Moonshot program), 1R01AI114581 from National Institute of Health, V2014-001 from the V-Foundation and 128436-RSG-15-180-01-LIB from the American Cancer Society (to RW).

Competing interests: M.R.B. currently is the president and CSO of Aminex Therapeutics Inc, which is a pharmaceutical start-up company that actively develops polyamine blocking agents. All other authors declare no conflict of interest.

Figures

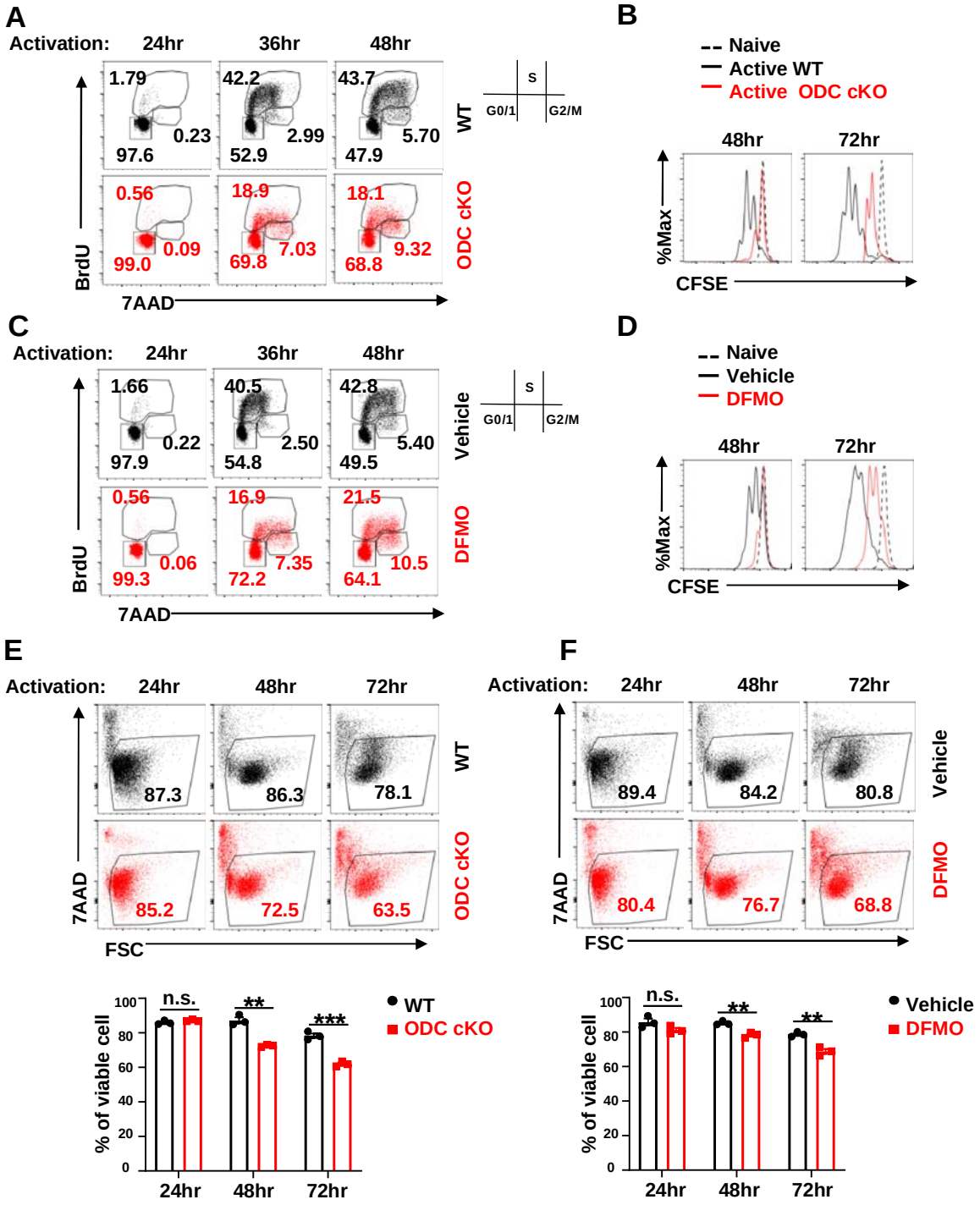

Figure 1. Blockage of de novo polyamine biosynthesis suppresses T cell proliferation and reduces viability *in vitro*.

689

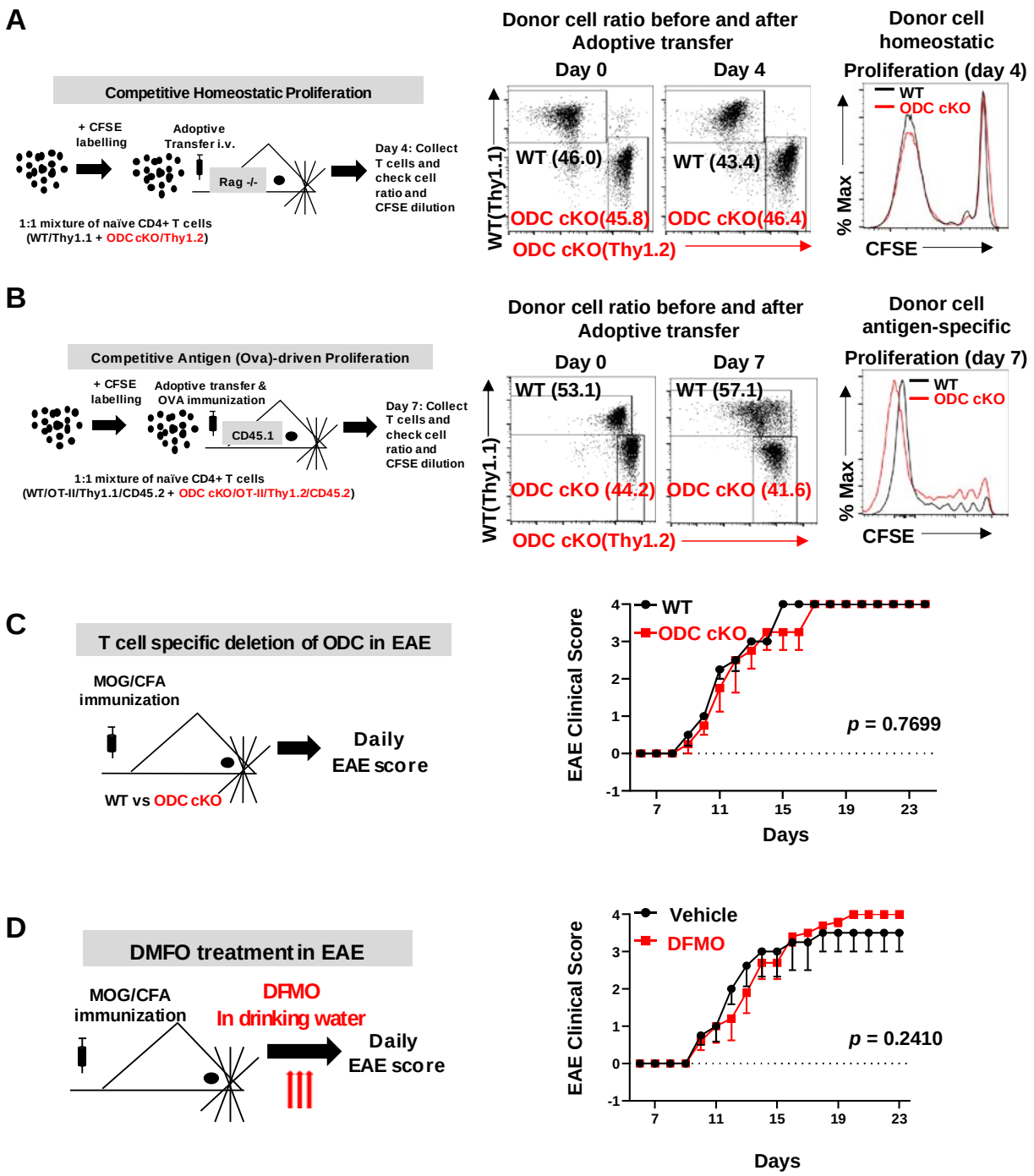

Figure 2. De novo polyamine biosynthesis is dispensable for driving T cell proliferation and function *in vivo*.

690

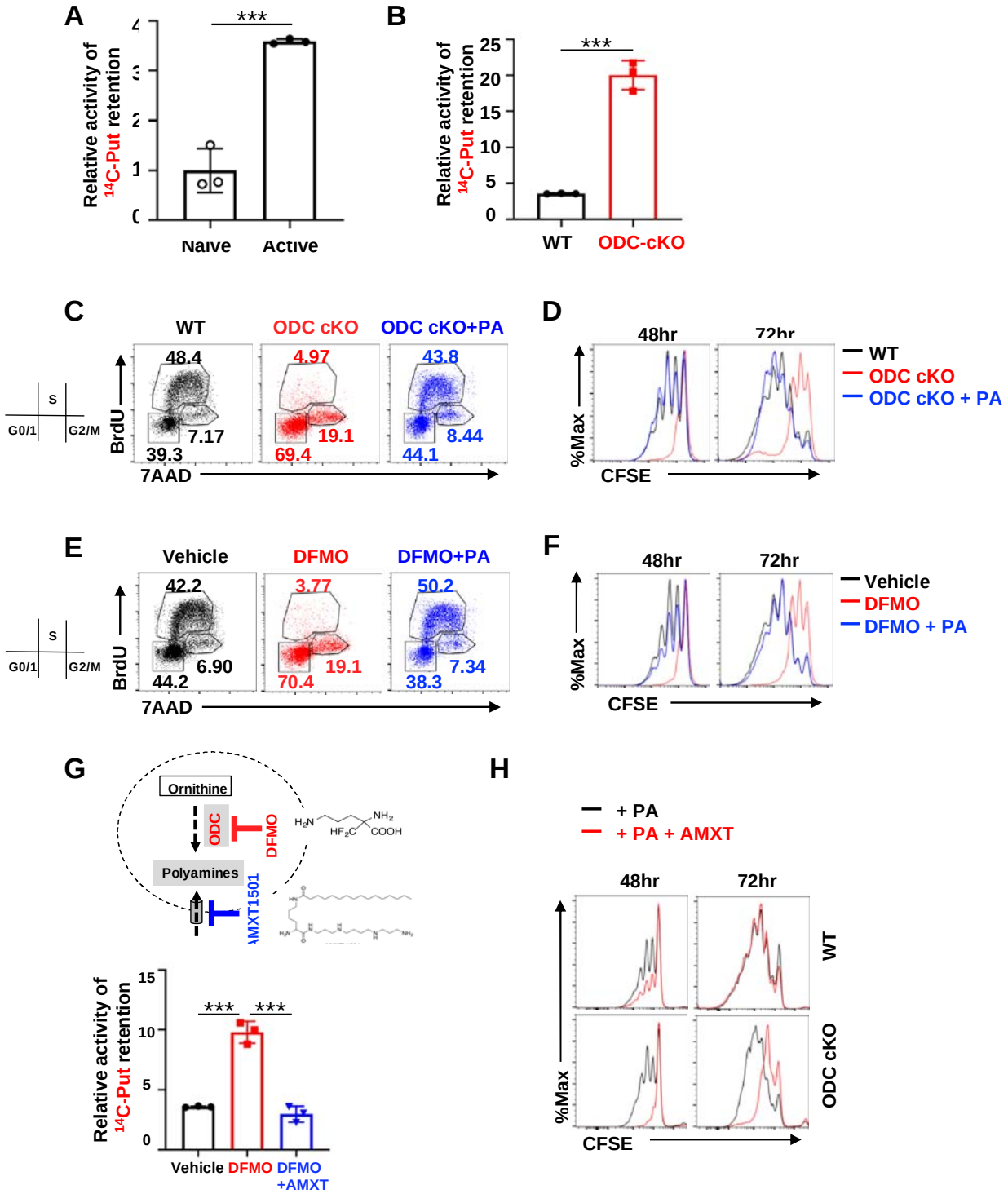

Figure 3. Ablation of de novo polyamine biosynthesis renders T cell dependent on polyamine uptake that can be blocked by AMXT 1501.

691

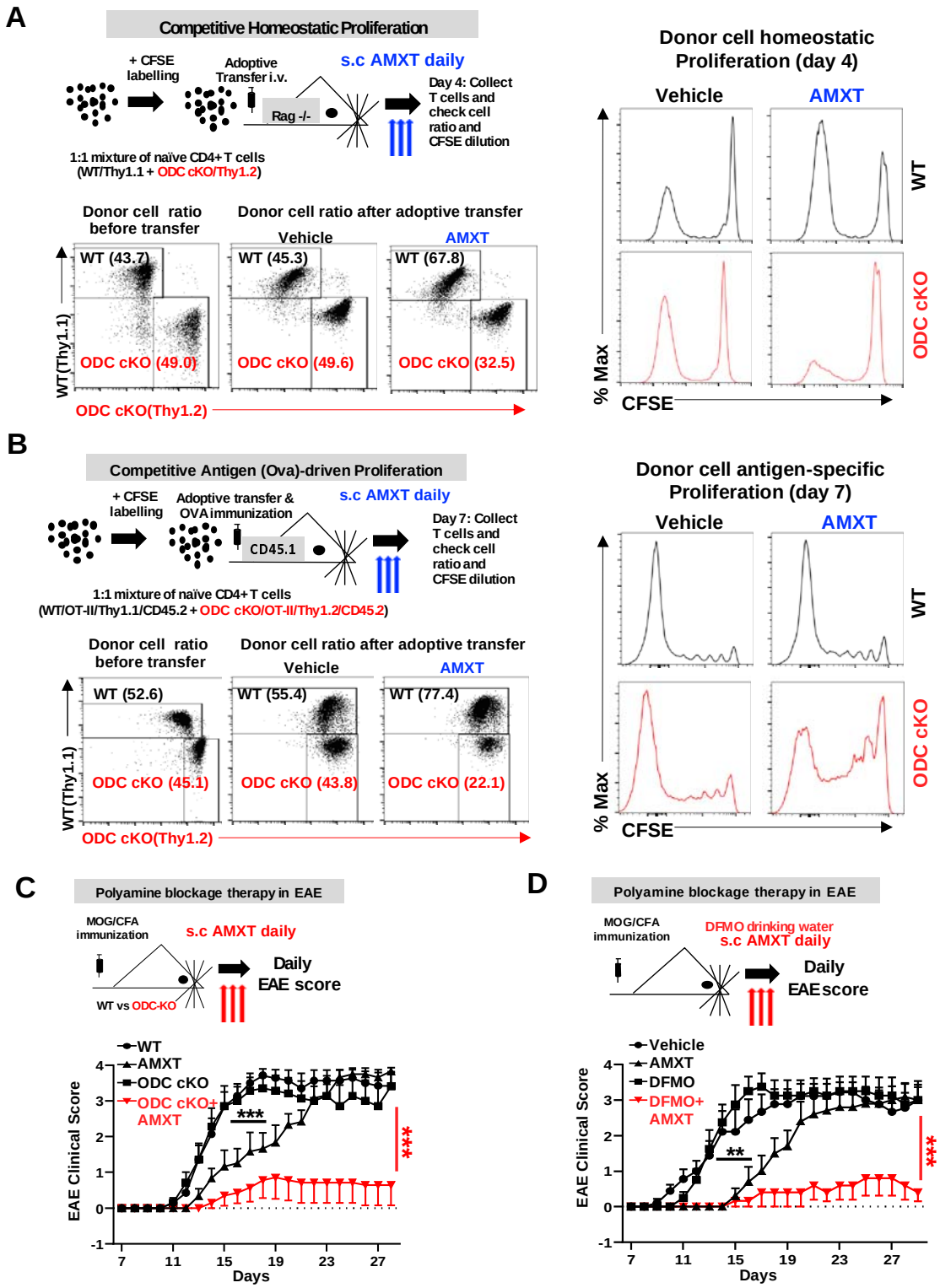

Figure 4. Simultaneous blockage of polyamine uptake and de novo biosynthesis suppresses T cell proliferation and function *in vivo*.

692

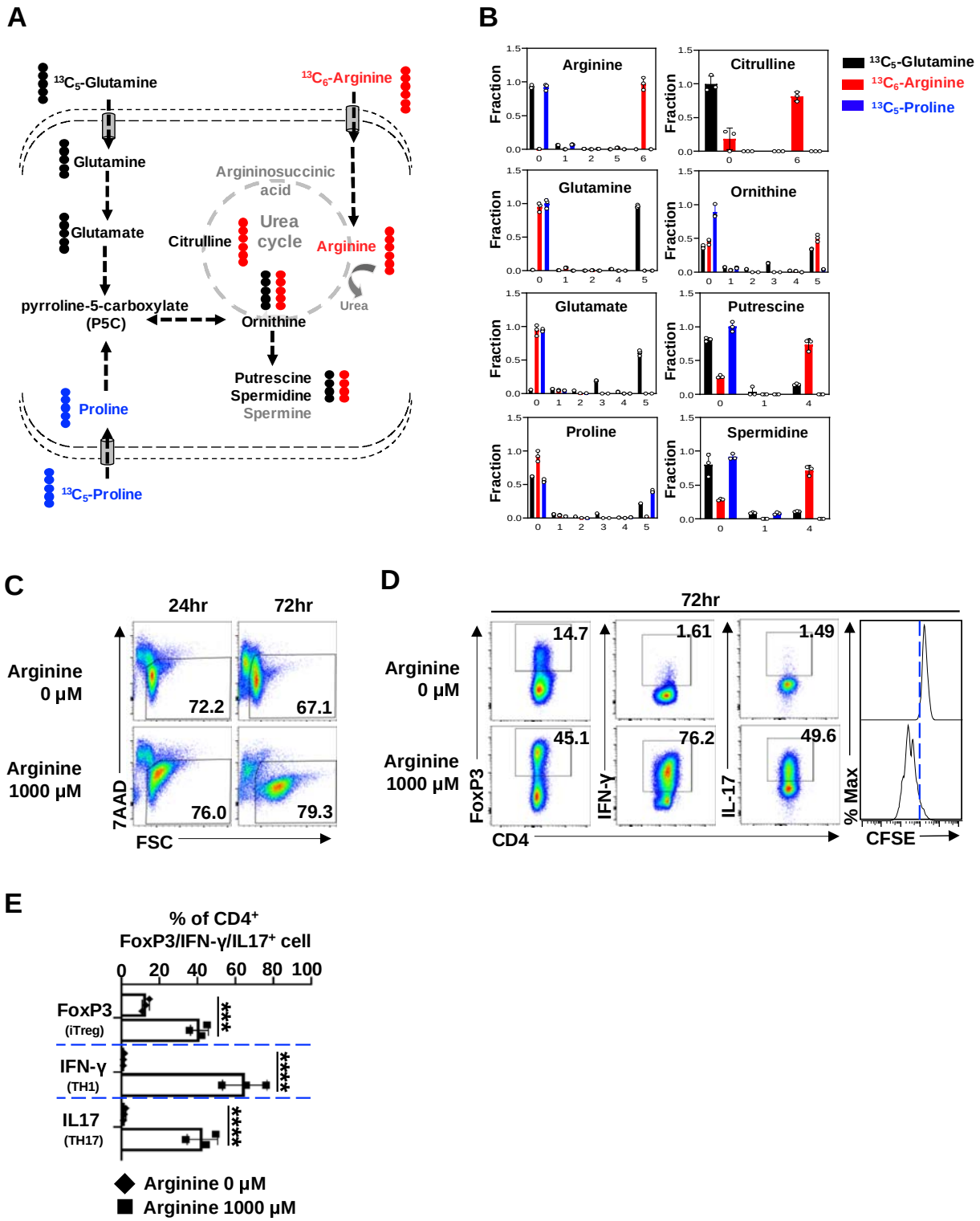

Figure 5. Arginine catabolism supports polyamine biosynthesis and T cell proliferation.

693

Figure 1. Blockage of de novo polyamine biosynthesis suppresses T cell proliferation and reduces viability *in vitro*. (**A and C**) Cell cycle of activated $CD4^+$ T cells at 24hr, 36hr and 48hr with indicated genotypes or treatments was analyzed by using BrdU and 7AAD staining, the numbers indicate the percentage of cells in each cell cycle stage. Data represent of 3 independent experiments. (**B and D**) Cell proliferation of naïve and activated $CD4^+$ T cells at 48hr and 72hr with indicated genotypes or treatments was determined by CFSE dilution. Data represent of 6 independent experiments. (**E and F**) Cell viability of activated $CD4^+$ T cells at 24hr, 48hr and 72hr with indicated genotypes or treatments was assessed by 7AAD staining. Top panel is the representative dot plot and bottom panel is the statistical analysis (mean ± SEM). Data represent of 3 independent experiments, $^{**}p < 0.01$, $^{***}p < 0.001$ compared with WT, one-way ANOVA.

Figure 2. De novo polyamine biosynthesis is dispensable for driving T cell proliferation and function *in vivo*. (**A and B**) An overview of *in vivo* competitive proliferation experimental procedure. The donor CD4 T cell ratios before and after adoptive transfer were evaluated by surface staining of isogenic markers, and cell proliferation was evaluated by CFSE dilution. Data represent of 3 independent experiments. (**C and D**) An overview of EAE experimental procedure. Clinical scores were evaluated daily (right panel). Data represent mean ± SEM (n=5) for each group, experiments were repeated 3 times.

Figure 3. Ablation of de novo polyamine biosynthesis renders T cells dependent on polyamine uptake that can be blocked by AMXT 1501. (**A, B and G**) Putrescine uptake in the indicated experimental groups was determined by the cellular retention of ^{14}C labeled putrescine

(mean ± SEM). Data represent of 3 independent experiments, $^{***}p < 0.001$, student's t-test. (**C and E**) Cell cycle of 48hr-activated $CD4^+$ T cells with indicated genotypes or treatments was assessed by using BrdU and 7AAD staining. The numbers indicate the percentage of cells in each cell cycle stage. Data represent of 3 independent experiments. (**D, F and H**) Cell proliferation of activated $CD4^+$ T cells at 48hr and 72hr with indicated genotypes or treatments was evaluated by CFSE dilution. Data represent of 3 independent experiments.

Figure 4. Simultaneous blockage of polyamine uptake and de novo biosynthesis suppresses T cell proliferation and function *in vivo*. (**A and B**) An overview of *in vivo* competitive homeostatic and antigen driven proliferation experimental procedure. The donor CD4+ T cell ratios before and after adoptive transfer were evaluated by surface staining of isogenic markers, and cell proliferation was evaluated by CFSE dilution. Data represent of 3 independent experiments. (**C and D**) An overview of EAE experimental procedure. Clinical scores were evaluated daily. Data represent mean ± SEM of n=5-10 for each group. Experiments were repeated 3 times.

Figure 5. Arginine catabolism supports polyamine biosynthesis and T cell proliferation. (**A**) Diagram of putative catabolic routes of $^{13}C_5$-Glutamine, $^{13}C_6$-Arginine, and $^{13}C_5$-Proline in T cells. (**B**) T cells were incubated in $^{13}C_5$-Glutamine or$^{13}C_6$-Arginine, or $^{13}C_5$-Proline medium for 36hr. Metabolites were extracted and analyzed using CE-TOFMS as described in methods. Numbers in the X-axis represent those of ^{13}C atoms in given metabolites. Data represent mean ± SEM of n=3 for each group. (**C**) Cell viability of activated $CD4^+$ T cell with indicated treatments

was determined by 7AAD staining. Data represent of 3 independent experiments. (**D and E**) $CD4^+$ T cells were activated and polarized toward iT_{reg}, T_H1 and T_H17 lineages with indicated treatment for 72hr. The indicated proteins were quantified by intracellular staining. Cell proliferation was determined by CFSE staining. Data represent of 3 independent experiments, $^{***}p < 0.001$, $^{****}p < 0.0001$, one-way ANOVA.

Supplementary Materials

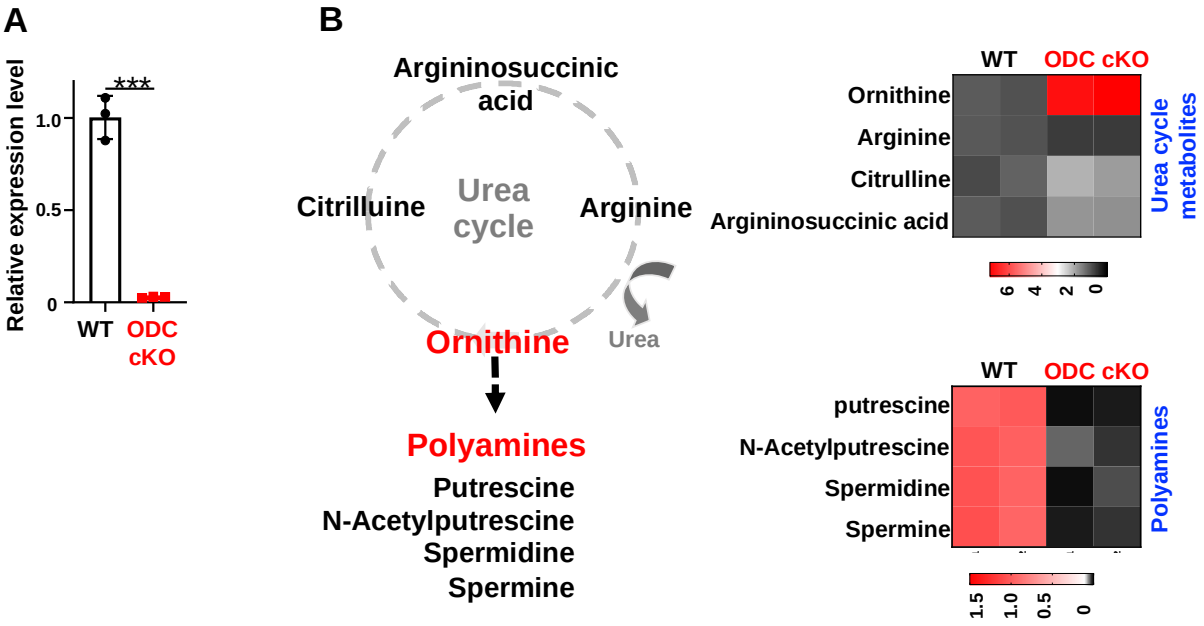

Supplemental figure 1. Genetic ablation of ODC disrupts the urea cycle and polyamine pool *in vitro*.

757

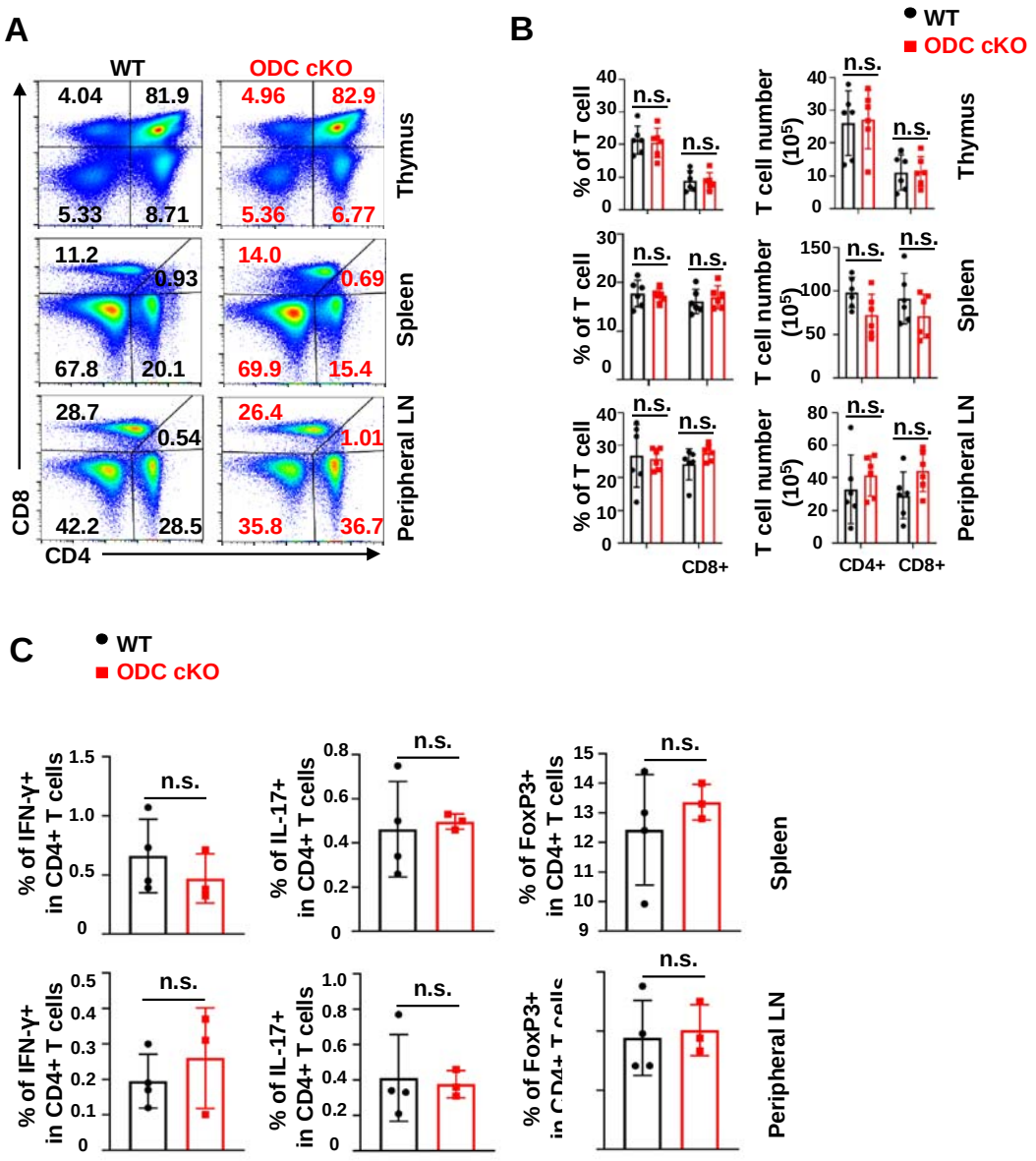

Supplemental figure 2. ODC-mediated de novo polyamine biosynthesis is dispensable for the development of mature T cells.

758

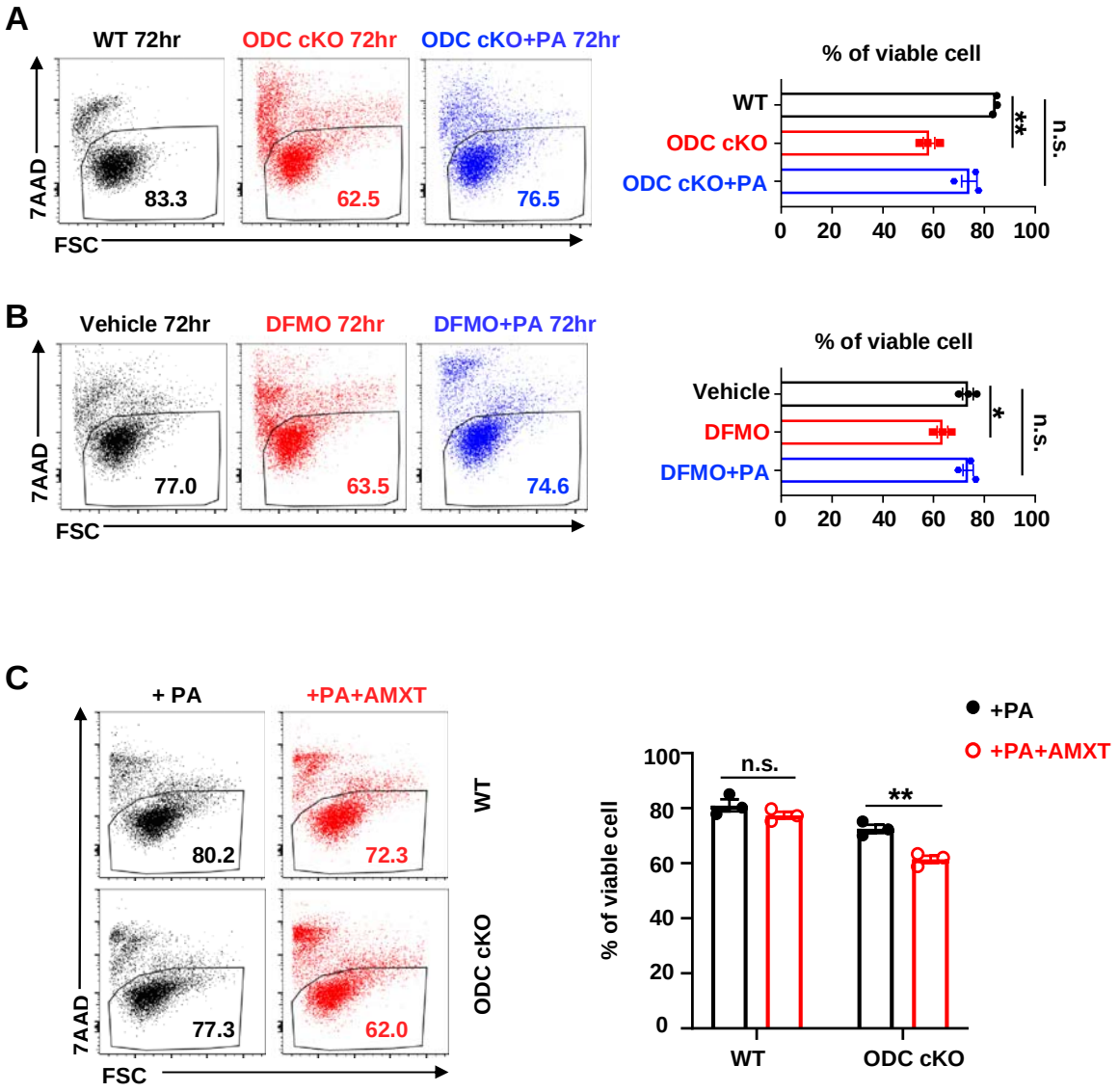

Supplemental Figure 3. Ablation of de novo polyamine biosynthesis renders T cell dependent on polyamine uptake for survival.

759

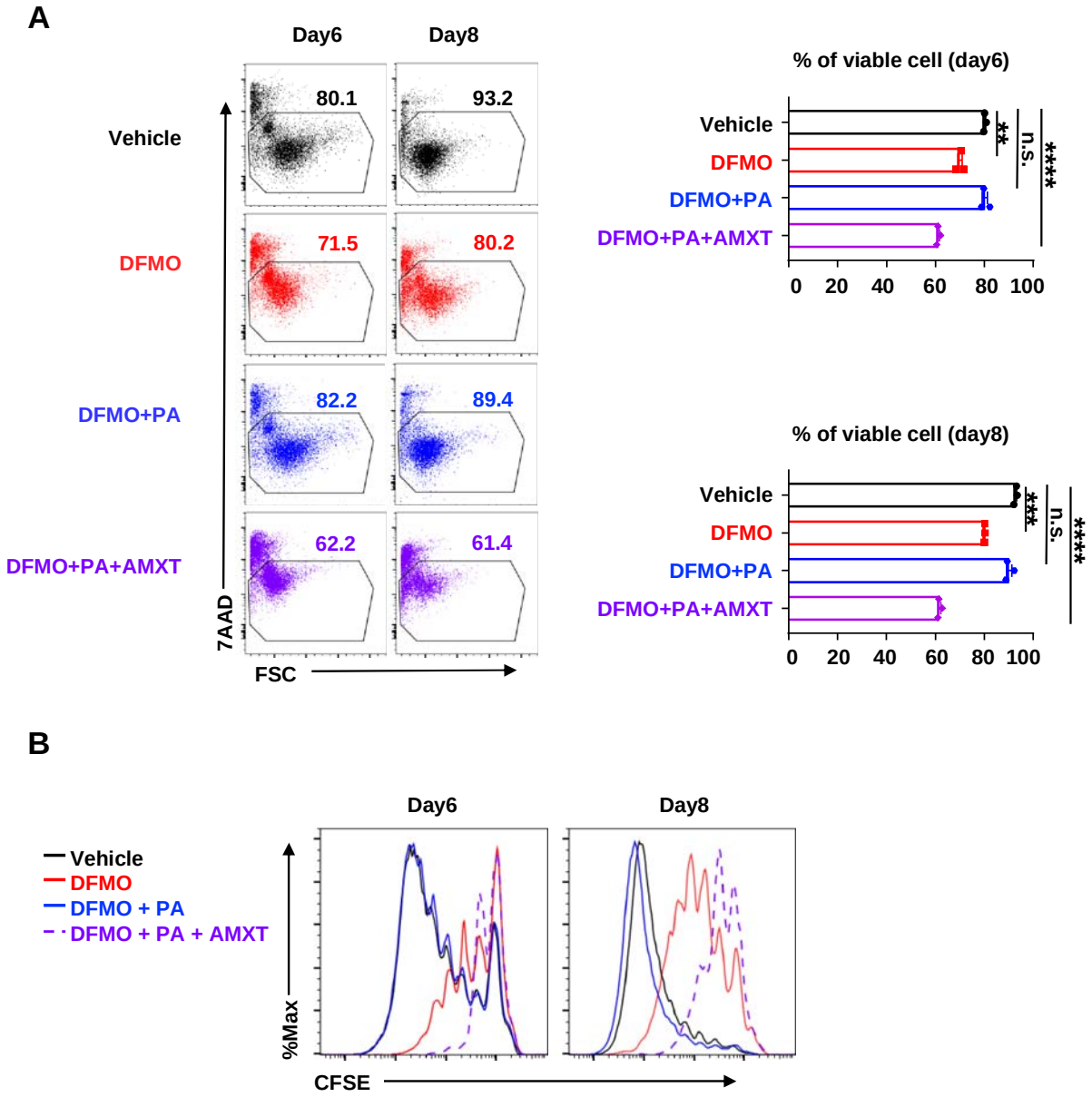

Supplemental Figure 4. Polyamine metabolism is required for human T cell proliferation and viability.

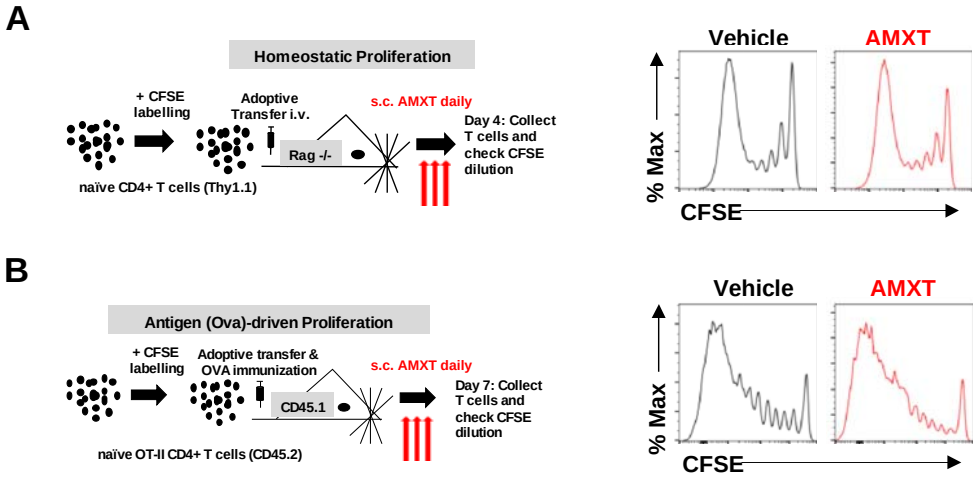

Supplemental Figure 5. AMXT treatment doesn't block T cell proliferation *in vivo*.

761

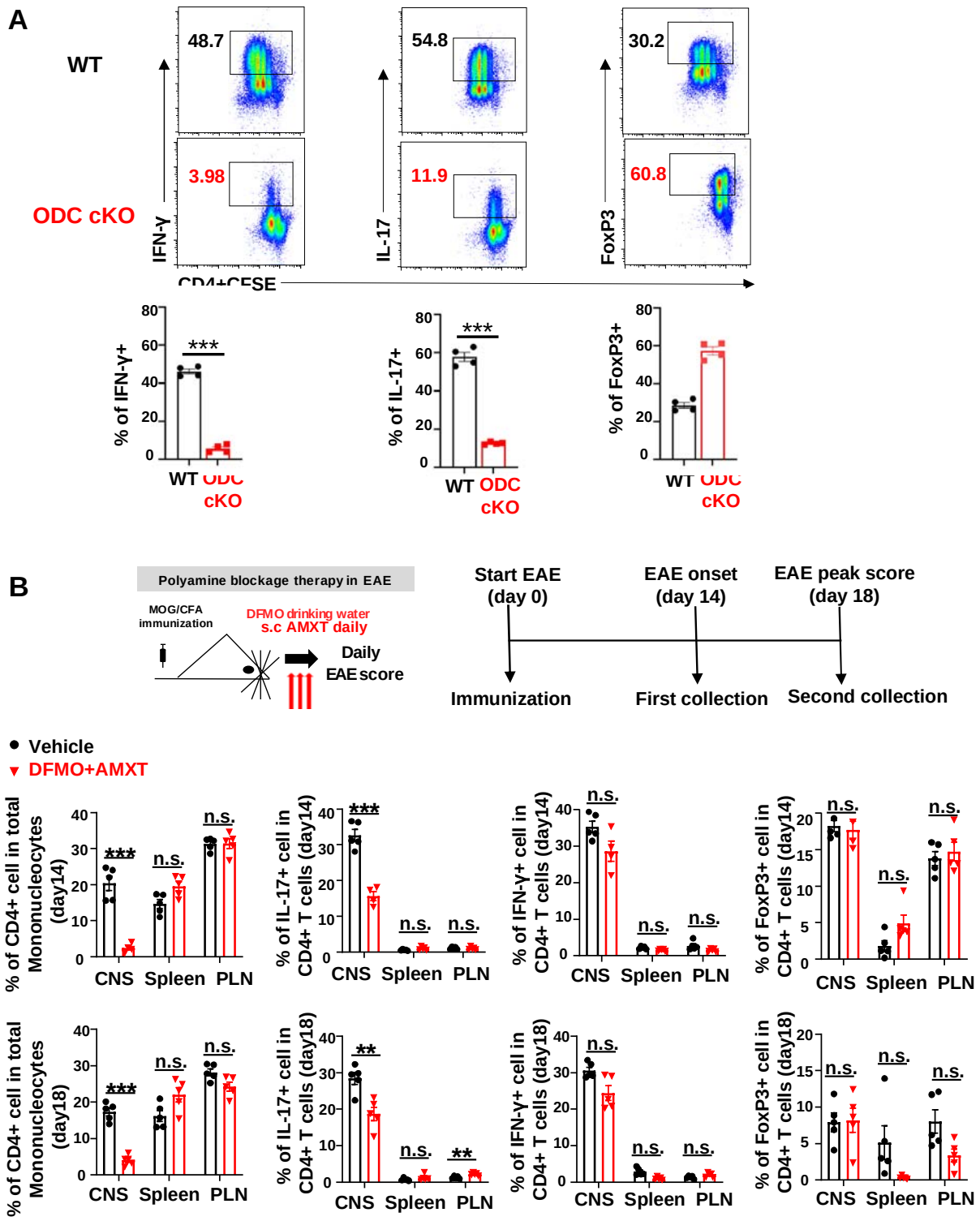

Supplemental Figure 6. Depletion of cellular polyamine suppresses pro-inflammatory T cell differentiation.

762

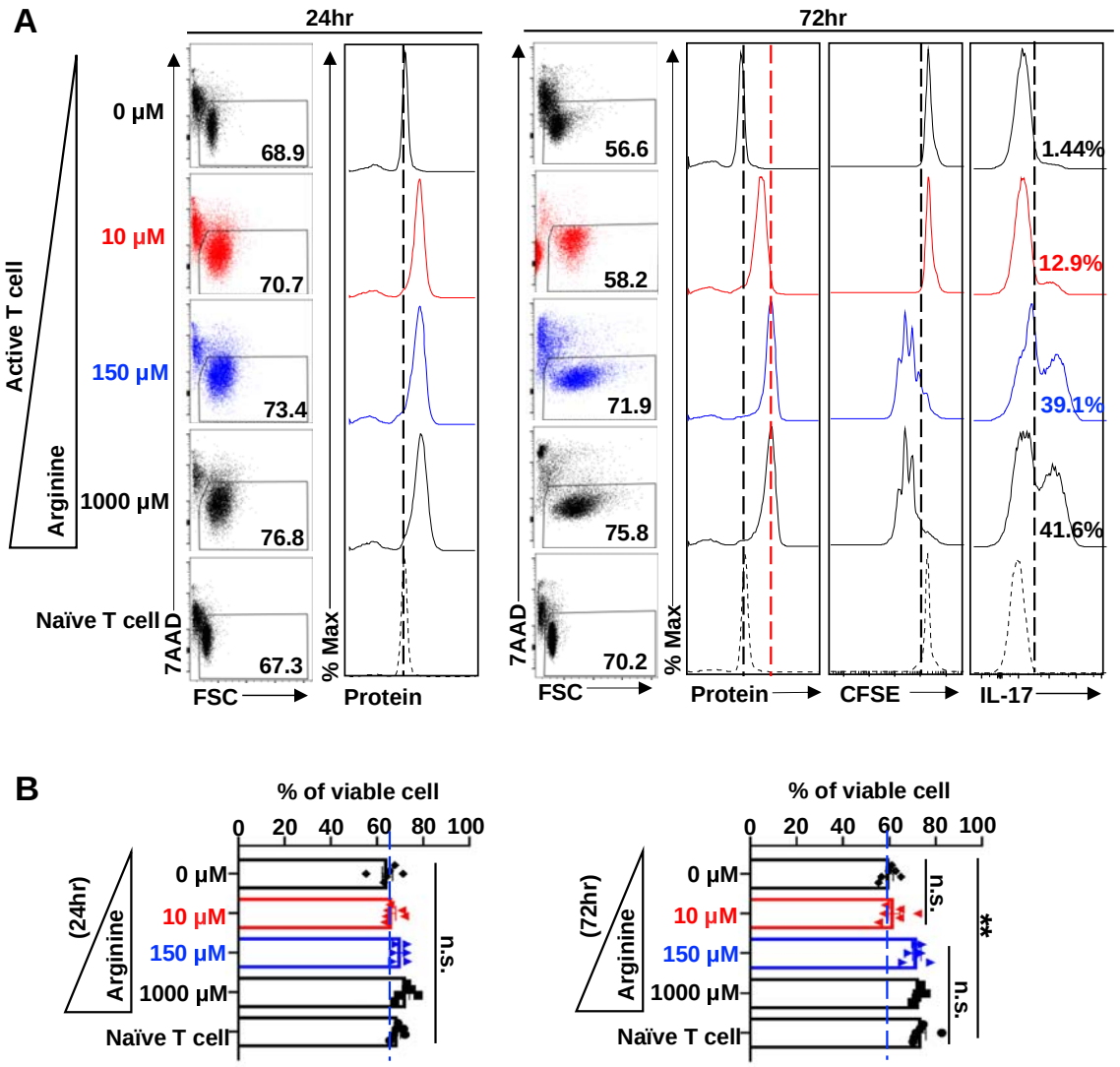

Supplemental Figure 7. The low level of arginine is insufficient to support cell proliferation and T_H17 differentiation.

763

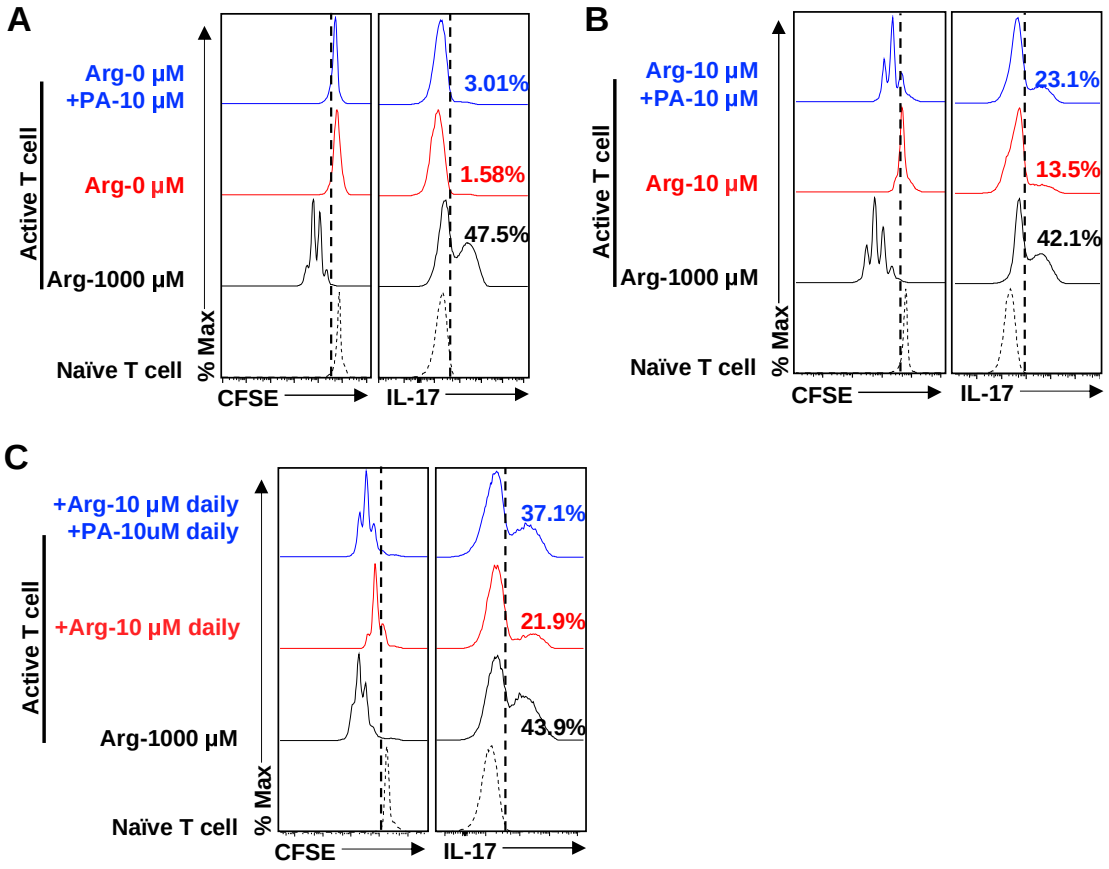

Supplemental Figure 8. Polyamine supplement renders T cell less dependent on arginine.

764

Supplemental Figure 1. Genetic ablation of ODC disrupts the urea cycle and polyamine pool *in vitro*. (**A**) ODC mRNA expression in activated T cells was determined by qPCR (mean ± SEM, n=3), $^{***}p < 0.001$. (**B**) Schematic view of polyamine de novo synthesis pathway through the urea cycle (left panel). Indicated metabolites in activated T cells were determined by CE-QqQ/TOFMS (right panel). Data represent of 3 independent experiments.

Supplemental Figure 2. ODC-mediated de novo polyamine biosynthesis is dispensable for the development of mature T cells. (**A-C**) Distribution of indicated T cell subsets in the thymus, spleen and peripheral lymph node (LN) were determined by cell surface and intracellular markers by flow cytometry (mean ± SEM, n=3-6). Data represent of 3 independent experiments.

Supplemental Figure 3. Ablation of de novo polyamine biosynthesis renders T cell dependent on polyamine uptake for survival. (**A-C**) Cell viability of activated $CD4^+$ T cells with indicated genotypes or treatments was assessed by 7AAD uptake (mean ± SEM). $^{**}p < 0.01$, $^{**}p < 0.05$, one-way ANOVA.

Supplemental Figure 4. Polyamine metabolism is required for human T cell proliferation and viability. (**A and B**) Human $CD4^+$ T ell viability and proliferation was evaluated by 7AAD uptake and CFSE dilution by flow cytometry. mean ± SEM. Data represent of 3 independent experiments, $^{**}p < 0.01$, one-way ANOVA.

Supplemental Figure 5. AMXT treatment doesn't block T cell proliferation *in vivo*. (**A and B**) An overview of *in vivo* proliferation experimental procedure. The donor T cell proliferation was evaluated by CFSE dilution. Data represent of 3 independent experiments.

Supplemental Figure 6. Depletion of cellular polyamine suppresses pro-inflammatory T cell differentiation. (A) Naïve $CD4^+$ T cells were activated under T_H1, T_H17 and iT_{reg} polarization conditions for 72hr. Indicated proteins were quantified by intracellular staining by flow cytometry. Data represent mean ± SEM of n=4 for each group, $^{***}p < 0.001$, student's t-test. **(B)** An overview of EAE experimental procedure. Cells were isolated from indicated organs, and indicated cell surface and intracellular proteins were quantified by flow cytometry. Data represent mean ± SEM of n=5 for each group, $^{**}p < 0.01$, $^{***}p < 0.001$, two-way ANOVA.

Supplemental Figure 7. The low level of arginine is insufficient to support cell proliferation and T_H17 differentiation. (**A**) Naïve $CD4^+$ T cells were activated under T_H17 polarization condition in the indicated conditional media. Cell viability, protein contents, proliferation and intracellular IL-17 levels were determined by flow cytometry. (**B**) Statistical analysis of cell viability in (**A**). Data represent of 6 independent experiments. $^{**}p < 0.01$, one-way ANOVA.

Supplemental Figure 8. Polyamine supplement renders T cell less dependent on arginine. (**A-C**) Naïve $CD4^+$ T cells were activated and differentiated under T_H17 polarized condition in the indicated conditional media. Cell proliferation and intercellular IL-17 expressions were determined by flow cytometry. Data represent of 3 independent experiments.

Supplemental Table 1. Hematological evaluation of AMXT 1501 and DFMO treatment in mice. Table S1.1-S1.5 Groups of 16 mice (1:1 Male/Female) were treated daily with the dose levels of AMXT 1501, DFMO or the combination shown in Table S1.1 for 28 days and analyzed for hematological parameters on day 29 (n = 5 mice, each sex), and after a 14-day recovery period on day 43 (n = 3, each sex). AMXT 1501 was delivered at the designated dose level by daily subcutaneous (s.c) injections. DFMO was delivered by daily oral gavage. Hematological

data on blood samples obtained at the time points noted were collected using an Advia 120 Hematology analyzer at Calvert Laboratories, Inc. (Scott Township, PA). Abbreviations used in study are summarized in Table S1.2. Data is shown in Tables S1.3 – S1.6.

Table S1.1: Treatment Groups for Hematology Response of AMXT 1501, DFMO and Combination in CD-1 mice.

Group	Number of animals	Dose Level AMXT 1501 (SC)	Dose Level DFMO (oral)
1*	16 (1:1 Male/Female)	0 mg/kg/day	0 mg/kg/day
2	16 (1:1 Male/Female)	2.5 mg/kg/day	0 mg/kg/day
3	16 (1:1 Male/Female)	5.0 mg/kg/day	0 mg/kg/day
4	16 (1:1 Male/Female)	10.0 mg/kg/day	0 mg/kg/day
5	16 (1:1 Male/Female)	2.5 mg/kg/day	200 mg/kg/day
6	16 (1:1 Male/Female)	5.0 mg/kg/day	200 mg/kg/day

*Control Group.

Table S1.2: Abbreviations used in study.

Abbr.	Description	Units
WBC	White Blood Cells	($x10^3$/mL)
RBC	Red Blood Cells	($x10^6$/mL)
HGB	Hemoglobin	(g/dL)
PLT	Platelets	($x10^3$/mL)
#LYMPH	Lymphocytes	($x10^3$/mL)
%LYMPH	% Lymphocytes	%
#MONO	Absolute Monocytes	($x10^3$/mL)
%MONO	% Monocytes	%
#NEUT	Absolute Neutrophils	($x10^3$/mL)
%NEUT	% Neutrophils	%

Table S1.3: Hematology Data – Males Day 29.

Group #		WBC ($x10^3$/mL)	RBC ($x10^6$/mL)	HGB (g/dL)	PLT ($x10^3$/mL)	#LYMPH ($x10^3$/mL)	%LYMPH (%)	#MONO ($x10^3$/mL)	%MONO (%)	#NEUT ($x10^3$/mL)	%NEUT (%)
1 (Control)	(n)	5	5	5	5	5	5	5	5	5	5
	Means	3.788	9.634	15.20	1085.4	2.684	70.46	0.120	3.20	0.654	17.10
	Sdevs	1.2549	0.8121	1.317	182.68	1.0170	14.223	0.0418	0.930	0.4794	9.276
2	(n)	5	5	5	5	5	5	5	5	5	5
	Means	4.396	9.386	14.70	1063.2	3.362	75.82	0.074	1.52*D	0.530	12.06
	Sdevs	1.7034	0.5033	0.992	101.86	1.3937	10.449	0.0713	0.909	0.3823	6.961
3	(n)	4	4	4	4	4	4	4	4	4	4
	Means	3.798	9.555	15.15	913.8	2.885	75.03	0.050	1.13+D	0.395	11.08
	Sdevs	1.0482	0.9829	1.060	104.11	0.9981	6.460	0.0497	1.031	0.0597	3.487
4	(n)	5	5	5	5	5	5	5	5	5	5
	Means	3.806	9.256	14.50	1372.0	2.312	60.08	0.070	1.76*D	0.906	23.04
	Sdevs	1.1046	0.4857	1.022	174.47	0.8287	11.861	0.0374	0.654	0.4133	4.618
5	(n)	5	5	5	5	5	5	5	5	5	5
	Means	4.266	10.058	15.68	970.0	3.202	75.24	0.086	2.04	0.636	15.08
	Sdevs	0.2840	0.3563	0.390	209.0	0.3330	7.561	0.0207	0.573	0.1971	5.112
6	(n)	5	5	5	5	5	5	5	5	5	5
	Means	4.582	9.804	15.46	1069.0	3.430	74.80	0.072	1.60*D	0.516	11.04
	Sdevs	0.8051	0.4598	0.532	275.15	0.8476	11.883	0.0286	0.596	0.1845	2.439

*D = Dunnett LSD Test Significant at the 0.05 level +D = Dunnett LSD Test Significant at the 0.01 level

Table S1.4: Hematology Data – Males Day 43.

Group #		WBC ($x10^3$/mL)	RBC ($x10^6$/mL)	HGB (g/dL)	PLT ($x10^3$/mL)	#LYMPH ($x10^3$/mL)	%LYMPH (%)	#MONO ($x10^3$/mL)	%MONO (%)	#NEUT ($x10^3$/mL)	%NEUT (%)
1 (Control)	(n)	3	3	3	3	3	3	3	3	3	3
	Means	4.127	9.553	15.07	1117.0	2.543	64.23	0.127	3.00	1.097	24.23
	Sdevs	1.4523	0.9238	0.833	354.53	0.6543	14.643	0,0723	0.755	0.8656	11.581
2	(n)	3	3	3	3	3	3	3	3	3	3
	Means	6.993	9.450	15.40	1035.0	5.427	76.43	0.170	2.23	0.983	14.57
	Sdevs	2.6921	0.1473	0.721	51.18	2.4413	6.558	0.1054	0.709	0.2663	2.136
3	(n)	3	3	3	3	3	3	3	3	3	3

	Means	5.280	9.923	15.60	1029.3	3.990	74.50	0.120	2.23	0.720	14.03
	Sdevs	1.2106	0.3859	0.529	185.40	1.3164	7.171	0.0458	0.306	0.1572	3.988
4	(n)	3	3	3	3	3	3	3	3	3	3
	Means	7.357	9.790	15.23	1087.0	5.780	78.10	0.170	2.23	0.883	11.93
	Sdevs	0.8931	0.2900	0.493	387.43	1.1391	5.851	0.0854	0.929	0.2108	2.301
5	(n)	3	3	3	3	3	3	3	3	3	3
	Means	5.680	10.127	15.37	1227.3	4.387	76.80	0.097	1.73	1.047	18.17
	Sdevs	2.3783	0.3774	0.643	57.24	1.9357	2.200	0.0551	0.462	0.4917	1.274
6	(n)	3	3	3	3	3	3	3	3	3	3
	Means	4.460	9.640	15.03	1239.7	3.483	78.23	0.070	1.50	0.723	16.17
	Sdevs	0.2762	0.9002	0.493	124.50	0.0971	2.658	0.0265	0.624	0.1607	3.134

*D = Dunnett LSD Test Significant at the 0.05 level +D = Dunnett LSD Test Significant at the 0.01 level

Table S1.5: Hematology Data – Females Day 29.

Group #		WBC ($x10^3$/mL)	RBC ($x10^6$/mL)	HGB (g/dL)	PLT ($x10^3$/mL)	#LYMPH ($x10^3$/mL)	%LYMPH (%)	#MONO ($x10^3$/mL)	%MONO (%)	#NEUT ($x10^3$/mL)	%NEUT (%)
1 (Control)	(n)	5	5	5	5	5	5	5	5	5	5
	Means	4.724	9.452	15.32	940.4	3.544	72.52	0.060	1.40	0.964	21.34
	Sdevs	1.9939	0.5288	0.572	71.00	1.6958	12.155	0.0474	0.894	0.5292	13.181
2	(n)	5	5	5	5	5	5	5	5	5	5
	Means	6.098	9.352	14.90	926.8	4.322	67.56	0.100	1.92	0.960	17.54
	Sdevs	2.7887	0.2511	0.663	189.98	2.2816	11.538	0.0515	0.988	0.3308	5.682
3	(n)	5	5	5	5	5	5	5	5	5	5
	Means	4.698	9.620	15.34	888.2	3.436	73.54	0.062	1.38	0.758	17.42
	Sdevs	2.2378	0.2185	0.321	149.78	1.6714	5.780	0.0396	0.593	0.2636	4.285
4	(n)	5	5	5	5	5	5	5	5	5	5
	Means	6.352	9.488	15.16	997.2	4.966	76.06	0.080	1.20	0.902	16.36
	Sdevs	2.7496	0.3942	0.336	149.83	2.4245	8.956	0.0828	1.175	0.2422	7.659
5	(n)	5	5	5	5	5	5	5	5	5	5
	Means	8.542	9.364	15.26	1026.2	7.040	81.70	0.118	1.54	0.942	11.46
	Sdevs	2.8356	0.5505	1.021	215.08	2.5584	2.927	0.0719	0.871	0.2214	1.705
6	(n)	5	5	5	5	5	5	5	5	5	5
	Means	8.632	9.600	15.34	844.6	6.822	78.06	0.186*D	1.62	1.168	14.74

	Sdevs	3.8693	0.4648	0.808	187.17	3.3188	7.474	0.0799	1.182	0.4640	5.092

*D = Dunnett LSD Test Significant at the 0.05 level +D = Dunnett LSD Test Significant at the 0.01 level

Table S1.6: Hematology Data – Females Day 43.

Group #		WBC ($x10^3$/mL)	RBC ($x10^6$/mL)	HGB (g/dL)	PLT ($x10^3$/mL)	#LYMPH ($x10^3$/mL)	%LYMPH (%)	#MONO ($x10^3$/mL)	%MONO (%)	#NEUT ($x10^3$/mL)	%NEUT (%)
1 (Control)	(n)	3	3	3	3	3	3	3	3	3	3
	Means	4.947	9.607	16.03	1031.0	3.687	71.33	0.077	1.40	0.900	21.27
	Sdevs	2.2258	0.0764	0.208	186.25	2.0033	10.753	0.0551	0.600	0.1054	10.179
2	(n)	3	3	3	3	3	3	3	3	3	3
	Means	4.357	9.590	15.63	1086.0	3.363	78.43	0.033	0.73	0.743	16.10
	Sdevs	1.2896	0.6110	0.709	354.37	0.7825	7.910	0.0351	0.643	0.4202	5.151
3	(n)	3	3	3	3	3	3	3	3	3	3
	Means	8.613	9.617	16.07	1058.7	6.410	73.33	0.123	1.43	1.177	13.63
	Sdevs	1.6946	0.3953	0.289	280.67	1.9048	9.047	0.0208	0.208	0.2511	0.666
4	(n)	3	3	3	3	3	3	3	3	3	3
	Means	7.943	9.813	15.70	903.3	6.363	80.00	0.167	2.10	0.883	11.57
	Sdevs	2.5551	0.2021	0.300	109.56	2.0938	2.152	0.0416	0.265	0.2248	2.723
5	(n)	3	3	3	3	3	3	3	3	3	3
	Means	5.103	9.477	15.57	1110.0	4.100	80.00	0.110	2.00	0.853	17.00
	Sdevs	1.6253	0.5450	0.702	190.59	1.4047	2.646	0.0889	1.00	0.2113	3.464
6	(n)	3	3	3	3	3	3	3	3	3	3
	Means	7.920	10.083	15.83	854.0	6.290	79.40	0.160	2.03	1.047	13.27
	Sdevs	0.1670	0.1002	0.306	260.87	0.0954	0.529	0.0100	0.058	0.1060	1.617

*D = Dunnett LSD Test Significant at the 0.05 level +D = Dunnett LSD Test Significant at the 0.01 level